

## RESEARCH ARTICLE

WILEY

# Quantifying modeling uncertainties in seismic analysis of dams: Insights from an international benchmark study

**Mohammad Amin Hariri-Ardebili**

College of Computer, Mathematical and Natural Sciences, University of Maryland, College Park, Maryland, USA

**Correspondence**

Mohammad Amin Hariri-Ardebili, College of Computer, Mathematical and Natural Sciences, University of Maryland, College Park, MD 20742-3281, USA. PREP Researcher, Earthquake Engineering Group, National Institute of Standards and Technology (NIST), Gaithersburg, MD, USA.

Email: [amin.hariri@nist.gov](mailto:amin.hariri@nist.gov)

**Abstract**

Advances in nonlinear dynamic analysis of dams have not completely resolved concerns over modeling confidence and analysis accuracy. Verification and validation offer accuracy assessment, but uncertainties persist during performance evaluation due to both epistemic (modeling) and aleatory (parametric) sources. Epistemic uncertainties arise from simplifications and modeling techniques. This paper addresses epistemic uncertainties in a gravity dam seismic analysis using data from the International Commission on Large Dams (ICOLD) benchmark study. While the benchmark formulation included the finite element model of the dam, mechanical material properties, and dynamic loads, participants retained the flexibility to opt for best-practice modeling assumptions, simplifications, and other specifics. Notable response variability emerged, particularly in crack profiles and damage predictions. This study examines sources of variability, quantifying modeling uncertainty for the benchmark problem. More specifically, the modeling variability is quantified using the logarithmic standard deviation, also known as dispersion. This metric enables its incorporation into other seismic risk assessment and fragility studies. Under relatively low-intensity motion (peak ground acceleration [PGA] of 0.18 g in this case), modeling dispersion of 0.45, 0.30, 0.32, and 0.30 were calculated for the maximum dynamic crest displacement, maximum hydrodynamic pressure at the heel, heel and crest maximum acceleration, respectively. Additionally, the dispersion of the failure PGA was determined to be 0.7. Findings underscore the need for systematic seismic response modeling in dam engineering to enhance prediction accuracy. A better understanding of the sources and magnitudes of modeling uncertainties can help improve the reliability of dam seismic analysis and contribute to the development of more effective risk assessment and mitigation strategies.

**KEYWORDS**

benchmark study, concrete dams, modeling variability, seismic analysis, uncertainty quantification

This is an open access article under the terms of the [Creative Commons Attribution-NonCommercial](https://creativecommons.org/licenses/by-nc/4.0/) License, which permits use, distribution and reproduction in any medium, provided the original work is properly cited and is not used for commercial purposes.

© 2023 The Authors. *Earthquake Engineering & Structural Dynamics* published by John Wiley & Sons Ltd.

## 1 | INTRODUCTION

The numerical simulation of engineered structures has perpetually posed challenges for analysts due to the numerous unknown parameters inherent in the modeling process. These uncertainties encompass various aspects, including modeling techniques of physical assets, the level of model fidelity, solution algorithms, loading definitions, material parameters, and more. Among engineering structures, dams hold a distinctive position owing to the intricacies entailed in their response. For instance, a concrete dam represents a massive concrete structure characterized by considerable heterogeneity across its various sections. Unlike building systems, the dam's response is significantly influenced by interactions with the foundation rock and the reservoir, rendering it a coupled system problem.<sup>1</sup> This coupling introduces an additional layer of complexity, as coupled system mechanics diverge from solid mechanics principles.

Within modern analysis procedures (and often in design contexts), verification, validation, and uncertainty quantification (UQ) stand as foundational components. Verification pertains to the mathematical accuracy of numerical solutions, while validation concerns the efficacy of mathematical models in emulating real-world systems.<sup>2</sup> UQ combines these facets with the inherent variability present in real-life systems to yield an overarching quantification of predictive uncertainty.<sup>3,4</sup>

In the realm of probabilistic analysis for structural models, UQ involves the “systematic study and reduction of uncertainties, both in computational simulations and real-world scenarios.” Its primary aim is to assess the likelihood of specific outcomes, accounting for incomplete knowledge about certain facets of the system.

In the field of Civil Engineering, the uncertainty classification framework introduced by [5] (Figure 1) is widely employed. This taxonomy categorizes uncertainties into abstracted uncertainties stemming from elements of the actual or modeled system, and cognitive uncertainties arising from subjective abstractions of reality. Engineers and analysts can conveniently classify uncertainties into abstracted and non-abstracted forms based on their expertise, background, and general knowledge of the system. Non-abstracted sources encompass physical randomness, vagueness, human and organizational errors, as well as information conflicts and confusion. The framework by [5] represents a classic and comprehensive classification widely adopted in Civil Engineering applications.

In dam engineering, a prominent historical challenge over the past three decades revolved around validating and verifying numerical models utilized for simulations, with limited emphasis on UQ until recently. Finite element<sup>1</sup> model validation and verification have been previously explored in the context of structural health monitoring,<sup>6</sup> and system identification frameworks,<sup>7</sup> encompassing both static and transient scenarios. While these methodologies offer insights into dam seismic response, fully validating and verifying a finite element model against an actual dam's behavior under earthquake ground motion remains a formidable task.

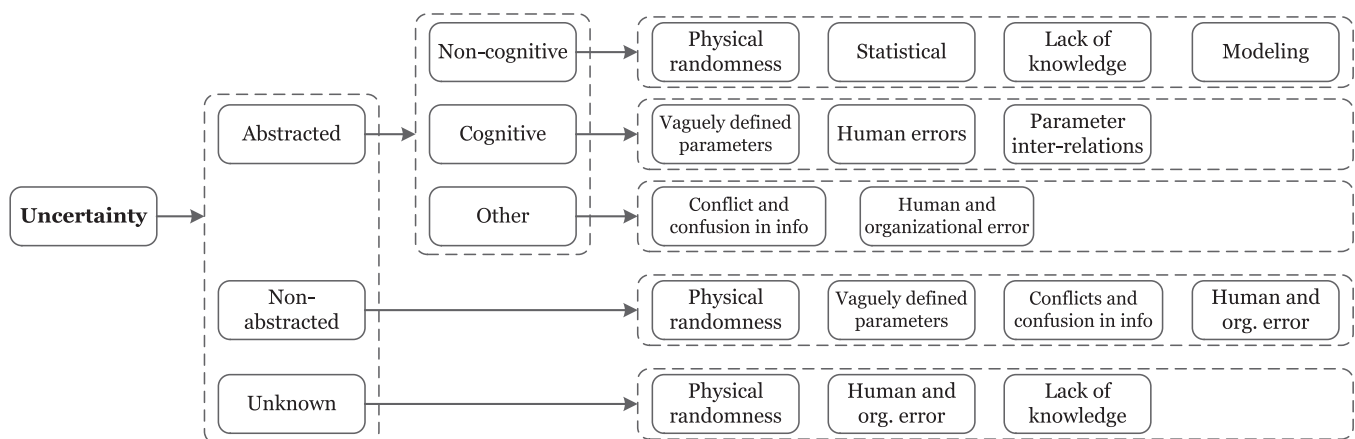


**FIGURE 1** Illustration of a comprehensive uncertainty classification in Civil Engineering, adapted from [5]. This taxonomy provides a structured framework for categorizing uncertainties, encompassing various aspects within the field.

<sup>1</sup> From here on, the term “finite element” will be used as a main substitute for “numerical modeling,” as the majority of dam structural analyses are conducted using the finite element method, with only a few accessible studies exploring finite difference, extended finite element, mesh-free, and other techniques.

Previous endeavors included shake table tests<sup>8</sup> as well as centrifuge tests<sup>9</sup> on small-scale dam models. In shake table tests, reduced-scale dam models are subjected to dynamic excitations based on similitude principles. However, these tests don't account for gravity effects on material behavior. Centrifuge testing, on the other hand, simulates the influence of high-speed rotation on dams, accounting for gravity's impact on material behavior. Dynamic centrifuge tests accurately reproduce the prototype stress field and mimic prototype material properties.

Hence, ensuring the fidelity of a developed finite element model to actual behavior entails cross-validation against published research, benchmark workshops, and blind prediction contests. Several instances of such cross-validation exist, including those organized by ICOLD and national organizations like USSD. A significant example is the 15th ICOLD International Benchmark Workshop<sup>10</sup> and the 2018 USSD benchmark workshop.<sup>11</sup> The author of this paper contributed to the formulation of both workshops and summarized their outcomes in reports. This paper's focus lies in highlighting the significance of addressing modeling uncertainties in seismic analysis of gravity dams, utilizing data collected from the 2019 ICOLD benchmark study in Italy. It is worth emphasizing that the field of finite element model UQ in concrete dams remains quite constrained, with only a handful of studies addressing this area.<sup>12–14</sup> These limitations primarily arise from the intricate nature of modeling the dam-foundation-water coupled system, a paucity of research efforts in this specialized field, limited benchmark studies, the computational intensity of resources required, scarcity of field and test data, insufficient standardization, the inherent variability and complexity of modeling theories (for example, distinct concrete damage models, diverse fluid-structure interaction (FSI) models, and various seismic wave propagation mechanisms in foundation rock), and a dearth of comprehensive knowledge among analysts.

The majority of published work in probabilistic assessment of dams has predominantly focused on material randomness and ground motion record-to-record (RTR) variability. In contrast, other disciplines within structural engineering have addressed the critical issue of modeling uncertainty. In a study by [15], uncertainties in construction details were incorporated on top of material properties randomness using a Bayesian framework. The findings revealed an increase in both the mean and standard deviation of the demand-to-capacity ratio for the structure. Similarly,<sup>16</sup> introduced uncertainty in the modeling of structures to assess the collapse risk of buildings. The inclusion of modeling uncertainty demonstrated an approximate 1.8-fold increase in the mean annual frequency of collapse compared to analyses neglecting modeling uncertainty, particularly for a high-seismic site. For models of reinforced concrete frames with infills,<sup>17</sup> incorporated uncertainty in the modeling parameters describing the nonlinear force-deformation response of equivalent infill struts. The study showed a shift in the median story drift ratio in the range of about  $\pm 20\%$ , while the dispersion increased by approximately 10–40% with the incorporation of modeling uncertainty. In the context of aging highway bridges,<sup>18</sup> incorporated a wide range of modeling-related uncertainties in fragility assessments. Their findings emphasized that the inclusion of only ground motion uncertainty is insufficient for this type of structure. Finally,<sup>19</sup> quantified the propagation of modeling parameter type uncertainty to the overall dispersion of the demand parameters. The mean ratio of the total dispersion to only RTR dispersion was found to be 1.27.

In the context of nonlinear seismic analysis applied to concrete dams, several factors contribute to modeling-related uncertainties. These include: (1) Variability in the chosen smeared crack model for concrete. (2) Variability in the discrete damage model applied to concrete and rock joints. (3) Challenges in translating measured material properties into constitutive models. (4) Variability in the FSI model. (5) Consideration or neglect of hydrodynamic pressure inside opened joints/cracks. (6) Uncertainty in the formulation of wave-absorbing boundary conditions for water and foundation's far-end. (7) Uncertainty in the formulation of wave propagation and soil-structure interaction. (8) Uncertainty in the aging model for concrete and its spatial distribution. (9) Consideration or neglect of pre-seismic loadings, such as stage construction, thermal loads, and long-term environmental loads. (10) Variability in different aspects of finite element modeling, including mesh size, time integration size and type (explicit or implicit solution), element type, element aspect ratio, convergence criteria and its threshold. (11) Consideration of geometric (large deformation) nonlinearity in the analysis. (12) The influence of human factors and the absence of proper quality control measures.

Benchmark problems and blind prediction exercises are commonly employed to assess the precision of numerical simulations and to quantify the extent of uncertainties in predictions. For example, the impact of modeling uncertainty on performance-based risk assessments has been systematically evaluated by researchers such as.<sup>20</sup> They utilized outcomes from the 7-story reinforced concrete building blind prediction contest to account for variations arising from software platforms, solution algorithms, element types, and model parameter computation or selection. In the context of structural and earthquake engineering, several benchmark exercises have been undertaken. Notable examples include blind prediction tests for the seismic evaluation of unreinforced masonry buildings,<sup>21</sup> shake table assessments of stone masonry building aggregates,<sup>22</sup> shake table testing of rocking podiums,<sup>23</sup> blind predictions of the seismic response of woodframe houses,<sup>24</sup> and a blind benchmark for the seismic assessment of slender masonry towers.<sup>25</sup>

This paper presents a pioneering effort in quantifying uncertainties related to modeling in nonlinear damage analysis of gravity dams. The primary objective is to establish a benchmark problem, subsequently identifying modeling uncertainties through collected information and quantifying their impact on structural response and dam failure. The ensuing sections will briefly discuss various sources of uncertainties within the context of concrete dam engineering, followed by an exploration of the case study and the information provided to participants. Subsequently, the assumptions made by different teams will be reviewed, along with a summarized presentation of results from around 20 papers. The quantity and nature of uncertainty in response will be quantified, and recommendations for future studies on nonlinear seismic dam analysis will be presented.

## 2 | CLASSIFICATION OF UNCERTAINTY SOURCES

The role of UQ holds paramount importance within probabilistic risk assessment frameworks,<sup>26</sup> a significance that magnifies when addressing critical structures<sup>27</sup> and complex systems like dams. Various classifications of uncertainty sources exist, each offering diverse perspectives. Here, several of these classifications will be examined.

One notable classification by [28] delineates uncertainty into three categories: (1) parameter uncertainty pertains to uncertainty in quantifying a model with a predetermined functional form, (2) modeling uncertainty encompasses the uncertainty surrounding the suitability of the structural or mathematical model's form, and (3) completeness uncertainty signifies the extent to which the model encompasses all phenomena relevant to the simulated system.

Another classification segregates variables into two fundamental categories: epistemic uncertainties and aleatory uncertainties.<sup>29</sup> Aleatory uncertainty, also referred to as objective uncertainty,<sup>30</sup> characterizes the inherent randomness of phenomena. In the context of seismic analysis for concrete dams, uncertainties linked to earthquake events (e.g., intensity, timing, and recurrence) assume paramount importance as significant uncertain parameters.<sup>31</sup> Aleatory uncertainty is commonly quantified through random variables (RVs) using the mathematical framework of probability theory.<sup>32</sup> Epistemic uncertainty, or subjective uncertainty, emerges from knowledge gaps. An instance is the uncertainty related to material properties, such as concrete fracture energy. This category encompasses various sources, including model and statistical uncertainty.<sup>33</sup> For continuous RVs, epistemic uncertainty can be quantified through probability density functions (PDFs).

### 2.1 | Ground motion RTR variability

Ground motion RTR variability is important in seismic evaluation of dams, arising from the unpredictability of earthquake events. Methods like Incremental Dynamic Analysis (IDA)<sup>34–36</sup> and Multiple Stripe Analysis (MSA)<sup>37–39</sup> account for RTR variability by utilizing scaled ground motion records, while the cloud analysis typically uses the un-scaled ground motion records.<sup>40–44</sup> Seismic fragility functions are valuable tools to convey the outcomes of extensive probabilistic seismic simulations,<sup>45</sup> and enhance the understanding of dam responses under varying seismic conditions.

### 2.2 | Material randomness

Material uncertainties significantly impact seismic analyses of dams. These uncertainties in mechanical properties of material are commonly modeled with statistical distributions. When multiple RVs are involved, accounting for correlations becomes essential. Multivariate correlations,<sup>46</sup> like  $\rho_{(E_c, f_c)}$ , and spatial correlations<sup>47</sup> are two important ingredients to precisely quantify material uncertainty in dam engineering.

### 2.3 | Modeling uncertainty

In the context of seismic analysis, the uncertainty in response modeling primarily stems from the inability of an idealized numerical model to precisely predict the actual behavior of an engineered system under the influence of ground motions.<sup>20</sup> elucidate that modeling uncertainty embodies the uncertainty linked to the model's efficacy in accurately representing the

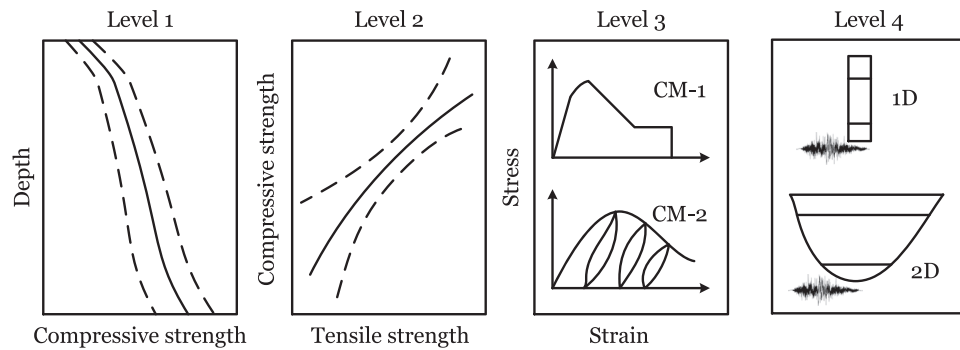


**FIGURE 2** Illustrative examples representing the four distinct types of modeling uncertainties in the context of seismic response analysis for concrete dams; Constitutive Model; Adapted from [48].

authentic structural response. However, Bradley<sup>48,49</sup> further extends this classification into the subsequent sub-categories, illustrated in Figure 2:

**Level 1 Uncertainty:** This category encompasses uncertainties in the measurement of physical quantities, such as the tensile strength of concrete or the estimation of soil shear stiffness. Level I uncertainty hinges solely on the quality of physical experiments and doesn't directly impact numerical model preparation. Nonetheless, since these measurements serve as input parameters in numerical simulations, they exert influence on the final response quantities.

**Level 2 Uncertainty:** In this tier, uncertainty arises from the correlation between measurable physical quantities and the constitutive model parameters. This form of uncertainty has been observed by researchers like.<sup>50–53</sup> For instance, while concrete compressive strength is commonly measured from core samplings, several constitutive models may necessitate knowledge of the tensile strength directly. As evident the level 2 modeling uncertainty is similar to material randomness discussed in Section 2.2.

**Level 3 Uncertainty:** This level encapsulates the uncertainty inherent in selecting a constitutive model, involving project-specific assumptions and simplifications.<sup>54,55</sup> Constitutive models are often crafted either empirically based on observations or theoretically derived via specific assumptions. In the context of concrete dams, a variety of options exist, such as fixed/rotating smeared crack models,<sup>56</sup> plasticity models,<sup>57</sup> damage mechanics models,<sup>58</sup> and fracture mechanics models,<sup>59</sup> to address concrete cracking and crushing during seismic loads.

**Level 4 Uncertainty:** This category involves uncertainty in the overall methodology of the idealized model. For instance, it encompasses decisions such as employing 3D models for dams with narrow valleys versus using 2D plane strain models.<sup>60</sup> Other examples include considerations like accounting for dam-foundation or dam-reservoir interactions, with potential fidelity differences. For dam-reservoir interaction, choices might involve using Westergaard hydrodynamic pressure or directly employing pressure-based fluid elements. Assumptions regarding boundary conditions, damping formulations, and ground motion input, including wave propagation assumptions, also contribute to this category.

### 3 | MULTIPLE UNCERTAINTY SOURCES

Uncertainty sources can be studied individually or collectively. The former approach examines independent epistemic and aleatory uncertainties (or other classifications like modeling and RTR variability), necessitating their adept integration to portray the complete uncertainty inherent in the system. The latter approach directly encompasses the correlations among various uncertainty sources, albeit often entailing higher computational expenses, particularly in simulation-based methods.

#### 3.1 | Decoupled aleatory and epistemic uncertainties

It is important to recognize that within the context of structural and earthquake engineering, a prevailing understanding suggests that the uncertainty arising from aleatory variables (particularly ground motion RTR variability) tends to outweigh the epistemic randomness (stemming from material and modeling variability). The stochastic nature of ground motion, coupled with its inherent unpredictability, and the possibility of calibrating incomplete information about



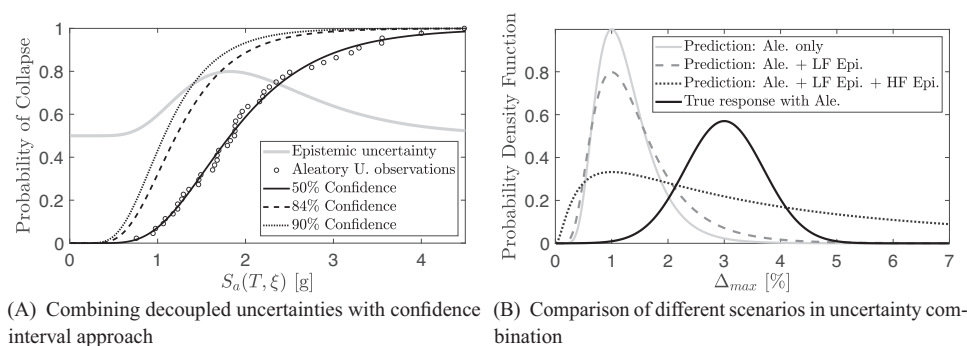


FIGURE 3 Accounting for multiple sources of uncertainties in seismic assessment of structural systems.

material and modeling randomness are the fundamental reasons for such a belief. As a result, the spread of results due to epistemic uncertainty is coupled with a model that explicitly addresses the effects of aleatory uncertainty. For instance, consider the case of a seismic fragility curve, which primarily hinges on aleatory uncertainty but incorporates adjustments for epistemic uncertainties.<sup>61</sup>

One approach to implementing this treatment is the confidence interval method.<sup>62,63</sup> Initially, the cumulative distribution function (CDF) of aleatory uncertainties is established using conventional techniques such as IDA or MSA. This results in a fragility curve with a median capacity denoted as  $\eta$  and an RTR dispersion designated as  $\beta_R$ . Subsequently, the PDF corresponding to the median of epistemic uncertainties is determined. This can be derived through diverse methods like expert judgment, First-Order Second-Moment, direct Monte Carlo simulations, and others. For simplicity, let's assume that the RV  $\eta$  follows a lognormal distribution<sup>2</sup>, with a median estimate of capacity denoted as  $\hat{\eta}$  and a dispersion labeled as  $\beta_U$ . The influence of epistemic uncertainty is incorporated by integrating the PDF with the median of the CDF. While the 50% confidence level (CL) aligns with a scenario featuring a sole aleatory uncertainty, the median capacity with CL confidence is defined as  $\eta^{CL} = \hat{\eta} \exp(-\beta_U \cdot K^{CL})$ , where  $K^{CL}$  is the standardized Gaussian variate associated with the probability  $CL$  of not being exceeded. Some of frequently used  $\{CL, K^{CL}\}$  combinations are:  $\{50\%, 0.00\}$ ,  $\{84\%, 1.00\}$ , and  $\{90\%, 1.28\}$ . To predict outcomes at a designated confidence level,  $CL$ , the aleatory distribution must be adjusted to the  $(1 - CL/100)$ th percentile of the epistemic distribution. Figure 3A illustrates hypothetical curves depicting 50%, 84%, and 90% confidence intervals.

### 3.2 | Integrated aleatory and epistemic uncertainties

The integration of uncertainty sources provides a more comprehensive depiction of the system, avoiding unwarranted assumptions in their amalgamation. Presently, a significant portion of combined uncertainty studies in dam engineering encompass material randomness and RTR variability, or address level 1 and 2 modeling uncertainties combined with RTR variability. However, relying solely on these simplified approaches (instead of more complex ones like levels 3 and 4 modeling uncertainties) can be problematic. Such simplified approaches consider uncertainties confined to material and model parameters within the constitutive model, disregarding the higher-fidelity uncertainties such as different constitutive models and modeling strategies.

Illustrated in Figure 3 are hypothetical scenarios wherein various uncertainty sources are combined at varying degrees of fidelity.<sup>49</sup> Three cases are examined, each showcasing the distribution of engineering demand parameters (EDP), for example, drift ratio: (1) a deterministic model with only aleatory uncertainty, (2) aleatory uncertainty integrated with low-fidelity epistemic uncertainties (akin to levels 1 and 2 in modeling uncertainty), and (3) aleatory uncertainty combined with both low- and high-fidelity epistemic uncertainties. While low-fidelity epistemic uncertainties may marginally augment system uncertainty (owing to model parameter uncertainty in simplified numerical models and predefined failure modes), the inclusion of high-fidelity sources of uncertainties (like constitutive model parameter

<sup>2</sup> The lognormal distribution is chosen due to its suitability for modeling positive RVs, a characteristic advantageous for parameters like material properties. Its skewness accommodates asymmetry in probability distributions, aligning well with uncertainties in structural and earthquake engineering, where factors such as material strength or damping may exhibit skewed behavior. Additionally, the logarithmic transformation simplifies multiplicative processes commonly encountered in material properties and structural responses.

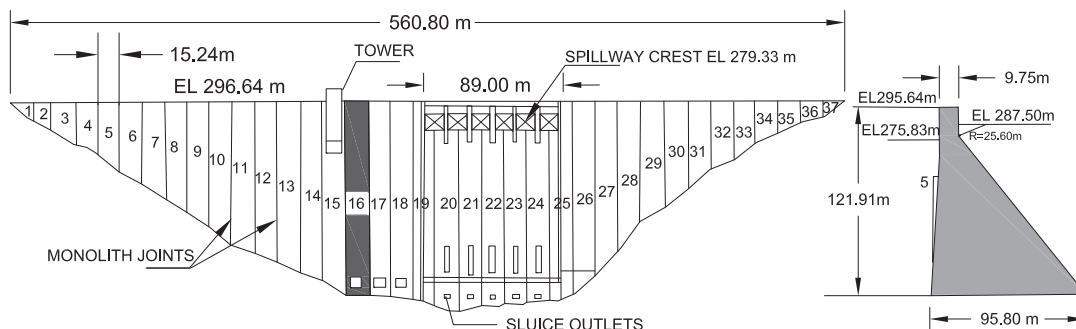


**FIGURE 4** Downstream view and cross-section geometry of monolith No. 16 of Pine Flat Dam; adapted from [72]. Both the 2D and 3D sliced finite element models of this cross-section are used for modeling UQ.

uncertainties) significantly amplifies system uncertainty. Low-fidelity models typically involve fewer unknown variables compared to high-fidelity models. For instance, consider the dam-foundation joint interface: a low-fidelity model might adopt the Mohr-Coulomb constitutive model, which comprises only two parameters (cohesion and friction angle). In contrast, a high-fidelity model might utilize a zero thickness, fracture mechanics inspired cohesive crack model with up to 14 parameters,<sup>64</sup> some of which are either practically challenging or very expensive to obtain through experimental tests. The increase in parameters in high-fidelity models, especially those associated with constitutive model parameters, contributes significantly to amplifying system uncertainty.

It is worth noting that these approaches might exhibit considerable bias when compared to the actual seismic performance of the system (that necessitates model validation and verification).

#### 4 | PROBLEM STATEMENT AND BENCHMARK DESCRIPTION

Considering the preceding discourse, which emphasizes that the most significant modeling uncertainty lies in the uncertainty associated with the model methodology itself, the omission of such modeling uncertainty raises a critical question: “Does the utilization of modeling technique, which overlook the majority of the fundamental physics underlying the problem, align with the principles of rigorous uncertainty analysis?”

To shed light on this query, this paper undertakes, for the first time, an examination of the outcomes from a meticulously structured benchmark workshop. The workshop design deliberately isolates the levels 3 and 4 modeling uncertainty sources by providing participants with comprehensive data. The benchmark problem encompasses an intricate dam geometry alongside its corresponding finite element mesh. Essential material mechanical properties for the mass concrete and foundation rock, including concrete strength and fracture parameters, as well as shear and compression wave velocities within the rock, are supplied. Notably, variations in reservoir water level corresponding to winter, summer, and normal pool conditions are detailed. The document explicitly outlines the requisite loading scenarios for the finite element simulation, encompassing seismic loads. Both seismic excitation at the free surface and its deconvolved version at the foundation base are furnished. Additionally, the benchmark includes recommendations for damping values and formulation.

By providing this extensive dataset to participants, the benchmark effectively eliminates ground motion RTR variability, material randomness, and levels 1 and 2 modeling uncertainties. Participants are granted the freedom to select any finite element software for analysis, explore diverse approaches for modeling the foundation and reservoir sections and their interactions with the dam, consider wave propagation complexities, implement various boundary conditions, opt for different numerical solvers (such as implicit or explicit methods), and decide on concrete constitutive models and damage behaviors, among other factors. These considerations collectively fall under the umbrella of levels 3 and 4 modeling uncertainties.

The case study is the tallest non-overflow monolith (#16) of Pine Flat Dam. Constructed by the US Army Corps of Engineers in 1954, this dam comprises 36 monoliths, of which 35 are 15.25 m-wide and 1 measures 12.2 m-wide. The dam extends linearly for a distance of 561 m and boasts a maximum height of 122 m in the case of the tallest non-overflow monolith, as depicted in Figure 4. Pine Flat Dam has been the subject of extensive study during the 1970s and 1980s at the University of California at Berkeley.<sup>65–71</sup> The reference coordinate system is situated at the dam heel and the mid-width of the monolith. The y-axis aligns with the downstream direction, while the z-axis points upward. It is assumed that the

**TABLE 1** Materials properties in the finite element model of Pine Flat Dam<sup>72</sup>.

	Parameter	Symbol	Unit	Quantity
Concrete	Modulus of elasticity	$E_c$	MPa	22,410
	Poisson's ratio	$\nu_c$	—	0.2
	Mass density	$\rho_c$	Kg/m <sup>3</sup>	2,483
	Compressive strength	$f_c$	MPa	28.0
	Tensile strength	$f_t$	MPa	2.0
	Fracture energy	$G_f$	N/m	250
	Compressive strain at peak load	$\epsilon_c$	—	0.0025
	Tensile strain at peak load	$\epsilon_t$	—	0.00012
Rock	Modulus of elasticity	$E_f$	MPa	22,410
	Poisson's ratio	$\nu_f$	—	0.33
	Mass density	$\rho_f$	Kg/m <sup>3</sup>	2,483
	Shear wave velocity	$V_S$	m/s	1,939
	Compressional wave velocity	$V_P$	m/s	3,167
Water	Mass density	$\rho_w$	Kg/m <sup>3</sup>	1,000
	compression wave velocity	$C_w$	m/s	1,439
	Winter water height	$L_W$	m	El. 268.21
	Summer water height	$L_S$	m	El. 278.57
	Normal water height	$L_N$	m	El. 290.00

dam-foundation interface is fully connected, thereby precluding any potential sliding. This assumption aligns with the benchmark's aim to streamline damage estimation using the continuum crack model. This deliberate choice enhances consistency and simplifies further UQ.

In the context of the nonlinear simulations discussed within this paper, the foundation block beneath the dam spans dimensions of 700 m by 122 m. Positioned 305 m from the left edge of the foundation block, the dam heel is located. Material properties, as outlined in Table 1, are presumed homogeneous and isotropic for both the concrete and rock components. Static load considerations encompass solely the weight of concrete and water. Participants were directed to incorporate viscous damping based on their prevailing comprehension, modeling conventions, and chosen analytical methods, with an expectation for thorough documentation.

The finite element model representing the dam–water–foundation rock system incorporates three primary contributors to energy dissipation: (1) material damping inherent in the concrete and rock; (2) radiation damping occurring in the semi-unbounded foundation and fluid domains; and (3) dissipation of hydrodynamic wave energy at the reservoir boundaries.<sup>73</sup> The modeling of material damping in both concrete and rock introduces significant uncertainty. The lack of experimental data on the energy-dissipating characteristics of concrete and rock under seismic loading conditions renders phenomenological modeling impractical.<sup>74</sup> Consequently, simplified viscous damping models are employed for their mathematical tractability. Radiation damping emerges as a predominant source of energy dissipation in 2D dam models, unless the foundation rock significantly exceeds the stiffness of the concrete.<sup>75</sup> However, for 3D dam models, this effect diminishes in significance.

In ICOLD workshop, for nonlinear simulations, participants were encouraged to explore the utilization of Rayleigh viscous damping, with a recommended value of 2% applied to both the dam and foundation. Based on a compilation of damping data from 32 concrete dams, obtained through forced vibration field tests and estimated from ambient vibration measurements,<sup>73</sup> demonstrated that damping levels range between 1% and 5%, spanning from the 10th to the 90th percentiles. Specifically, for Pine Flat Dam, damping was measured in the range of 2% to 3.5%.

Two distinct types of loads were furnished for the purpose of nonlinear transient simulations: a real ground motion record and an artificially generated acceleration profile. The real acceleration data employed originates from the M 7.3 Kern County, California earthquake on July 21, 1952, recorded at the Lincoln School in Taft. Specifically, only the S69E component of this ground motion was considered, with a peak ground acceleration (PGA) value of 0.18 g. The selection of the Taft ground motion, originally utilized in frequency-domain linear elastic analysis by Chopra et al.<sup>66–68</sup> for Pine Flat Dam, serves the purpose of facilitating model calibration. By allowing participants to compare their simulation



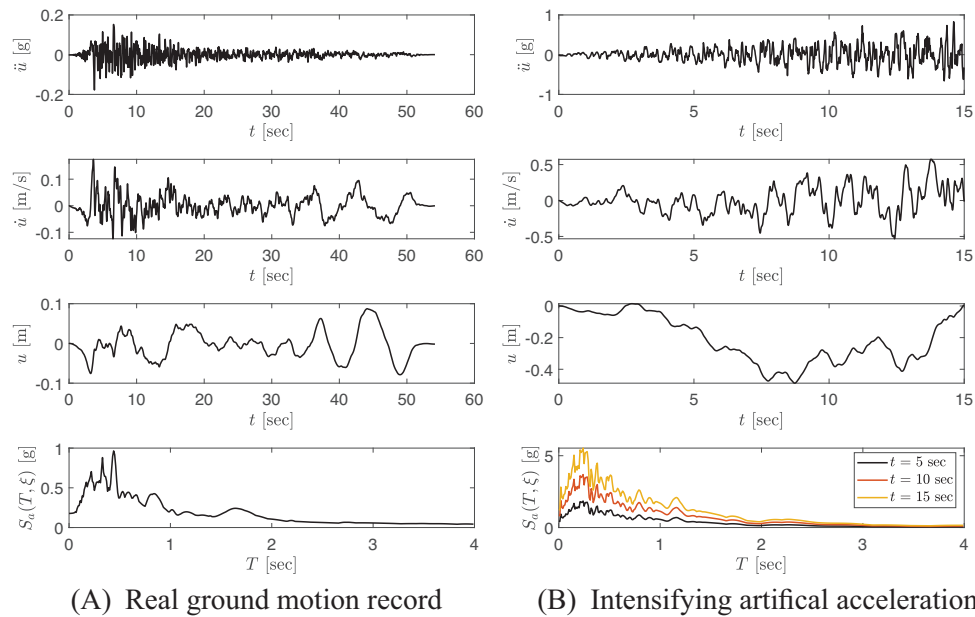


**FIGURE 5** Acceleration, velocity, and displacement time histories, along with the response spectrum of the input excitation. Note that the response spectrum is presented for the entire duration of real ground motion, whereas it is time-dependent in the case of IAA.

results, particularly in the linear elastic domain, with previous studies, the benchmark aims to mitigate potential bias in probabilistic simulations arising from substantial errors in one participant's predictions.

Given the assumption that this signal represents free surface conditions, its deconvolved counterpart is also included. The deconvolution procedure assumes a vertically-propagating SH-wave within a uniform half-space characterized by the same material properties as the foundation. Importantly, in the context of a free surface signal, the motion is assumed to be recorded at the top of the foundation in the absence of the dam and reservoir. Consequently, the free-surface motions are suitable for input in massless foundation models, whereas the deconvolved signals are intended for employment in massed foundation models. The significance of deconvolving seismic waves using both frequency- and time-domain approaches, along with a detailed implementation in the analysis of dam-foundation coupled systems, is extensively discussed in [76, 77]. Figure 5A illustrates the acceleration, velocity, displacement, and force time histories of the Taft ground motion, accompanied by the 2% acceleration response spectrum.

The second signal constitutes an intensifying artificial acceleration (IAA) function. Such artificial accelerations are generated through unconstrained optimization techniques<sup>78</sup> with a near-linear increase in peak acceleration and response spectrum over time. This methodology can be likened to a dynamic pushover procedure, which assesses the seismic performance of a dam across the spectrum from linear elastic behavior to nonlinear response, ultimately capturing theoretical collapse. Figure 5B provides an illustration of the provided IAA to participants, showcasing its associated velocity, displacement, and force time histories. Furthermore, acceleration response spectra are depicted at three distinct time points (5, 10, and 15 s). For further insights into the concept and application of IAA in dam engineering, refer to [79–83]. Validation of IAA with respect to classical IDA has been discussed in [84, 85].

## 5 | ANALYSIS AND SYNTHESIS OF RESULTS

This section presents a concise overview of the outcomes obtained from both real ground motion records and artificial accelerations. The following scalar and vector quantities were analyzed: crest and heel displacements, relative crest displacement compared to heel, net hydrodynamic pressure at the dam's heel, ratio of crest-to-heel amplitude acceleration spectrum, crack profile, area-based and length-based damage index (DI), and failure time (for IAA only). The data analyzed in this paper is derived from the findings presented in the following publications.<sup>86–104</sup> Table 2 provides an overview of key modeling variations observed across each study. These modeling variabilities encompass factors such as mesh type (2D, 3D slice, full 3D), mesh size (which holds significance for DI assessment), time step utilized in the numerical simulation, criteria for convergence, the specific foundation model and its associated boundary conditions for wave propagation

T A B L E 2 Summary of the modeling choices and variabilities by different participants.

ID	Mesh type	Mesh size [m]	Time step	Convergence criteria	Foundation type and boundary conditions	Fluid-structure interaction	Concrete constitutive (damage) model	Time integration	Software
11	2D plane strain	2		Norm of unbalance force	Domain reduction method with absorbing damping layers; No free-field BC	Finite volume mesh for fluid; compressible; acoustic-structural coupling		Implicit (solid); explicit (fluid coupling)	Real ESSI
12	2D plane strain	2.5–5.0	0.01	1%	Perfectly matched layers; Free-field BC only on the bottom of foundation	Incompressible fluid; acoustic-structure interaction	Total strain-based crack model with fixed-crack orientation including linear tensile curve	Explicit	Diana
13	2D plane strain	10	0.001	0.0001	Viscous-spring boundaries with massed foundation; With free-field BC	Compressible fluid; acoustic-structure interaction	Anisotropic damage model for pre-peak and orthotropic damage following Rankine criteria for post-peak; Isotropic damage under compression stresses using Drucker-Prager criteria	Implicit	Code-Aster
14	3D slice	2	0.01	Newton Raphson (Force)	Foundation bottom is kinematically constrained (Infinite radiation boundary); No free-field BC	Compressible fluid; acoustic-structure interaction	Drucker-Prager constitutive model with perfect plasticity	Explicit (Newmark)	Ansys
15	2D plane strain	1	0.01	Newmark	Simple supports; No free-field BC	Incompressible fluid; FSI with links-gap method	Concrete material in SAP with nonlinear properties	Explicit (Newmark and Linear)	Sap2000
16	3D slice	1.5	0.005	Nodal unbalanced forces	Viscous-spring artificial boundaries model with massed foundation; With free-field BC	Compressible fluid; acoustic-structure interaction	Concrete damage plasticity	Implicit (HHT)	Abaqus
17	2D plane strain	3	0.00005		Non-reflecting viscous boundary with free-field conditions at the lateral boundaries	Lagrangian displacement-based fluid with rotational penalty constraint; FSI	Discrete crack model with a bi-linear softening model in the normal and shear directions and Rokugo curve	Explicit (central difference)	DAMFA2D
18	2D plane strain	3	0.002	Hilber-Hughes-Taylor ( $\alpha = -0.3$ )	Non-reflecting boundary conditions using particular interface element characterized by a very low stiffness and damping coefficient; No free-field BC	Compressible fluid; acoustic-structure interaction	Crack width by multiplying elemental crack strain and the crack bandwidth (set to 0.5 m)	Implicit (HHT)	Diana
19	2D plane strain	15	0.001	First vibration frequency	Linear paraxial absorbing boundary elements; With free-field BC	Both acoustic fluid and Westergaard's added mass; FSI	Equivalent linearization technique (tensile-strain controlled)	Implicit (Newmark)	Code-Aster
20	2D plane strain	1.5	0.01	Packed scheme: moderate dissipation	Infinite element; With free-field BC	Compressible fluid; acoustic-structure interaction	Concrete damaged plasticity	Implicit (Direct)	Abaqus

(Continues)

TABLE 2 (Continued)

ID	Mesh type	Mesh size [m]	Time step	Convergence criteria	Foundation type and boundary conditions	Fluid-structure interaction	Concrete constitutive (damage) model	Time integration	Software
21	3D slice	1.0–37.0	0.01	Relative convergence criterion: 10 <sup>−6</sup>	Fixed BC for massless model; No absorbing BC	Added mass and acoustic fluid	Nonlinear tensile behavior only	Implicit (Newton)	Code-Aster
23	2D plane strain	0.5–4.0	0.005	5% for force and moment, 0.01% for mass flow rate, 5% for displacement	Viscous-spring boundary condition; No free-field BC	Compressible fluid; acoustic-structure interaction	Coupled damage-plasticity model based on micro-plane formulation	Implicit	Ansys
24	3D slice	1.4	0.00000567		Viscous boundaries (Lysmer); Free-field elements for lateral boundaries only	Compressible fluid with mixed discretization scheme	Elastic perfectly plastic constitutive law for shear with Mohr-Coulomb failure criterion; elastic perfectly fragile constitutive law for tensile	Explicit	Flac3D
26	2D plane strain	1	0.01	Energy based	Infinite elements with free-field BC based on Lysmer	Compressible fluid; acoustic-structure interaction	Concrete damage plasticity	Implicit	Abaqus
27	3D slice	3	0.0001		Viscous boundary conditions proposed by Lysmer; With free-field BC	Lagrangian displacement-based fluid with only normal stiffness; FSI	Bi-linear softening model in tension and shear with Rokugo curve	Explicit (Central difference)	Parmac3D
28	2D plane strain	1.5	0.01		Lysmer boundary condition; With free-field BC	Compressible fluid; acoustic-structure interaction	Concrete damage plasticity	Implicit	Abaqus
29	2D plane strain	2.5	0.01		Viscous spring elements; No free-field BC	Compressible fluid; acoustic-structure interaction	Concrete plasticity with Menetrey-William criterion	Implicit	Ansys
30	2D plane strain	3.5			Infinite elements; free field rock-column and direct free field forces	Compressible fluid; acoustic-structure interaction	Concrete damage plasticity	Implicit	Abaqus
31	2D plane strain	1.5	0.001		Viscoelastic artificial boundary; No free-field BC	Compressible fluid; acoustic-structure interaction	Concrete damage plasticity	Implicit	Abaqus
32	3d slice	10	0.01	Tolerance for largest nodal value available in the system + energy norm	Non-reflecting BCs with damper elements	Compressible fluid-like structural elements; FSI	Concrete material according to EN norms	Wilson theta	SOFISTIK
33	Plane Strain	3	6 <sup>−4</sup> to 0.01	Force equilibrium	Infinite elements; No free-field BC	Compressible fluid; acoustic-structure interaction	Concrete damage plasticity	Implicit	Abaqus

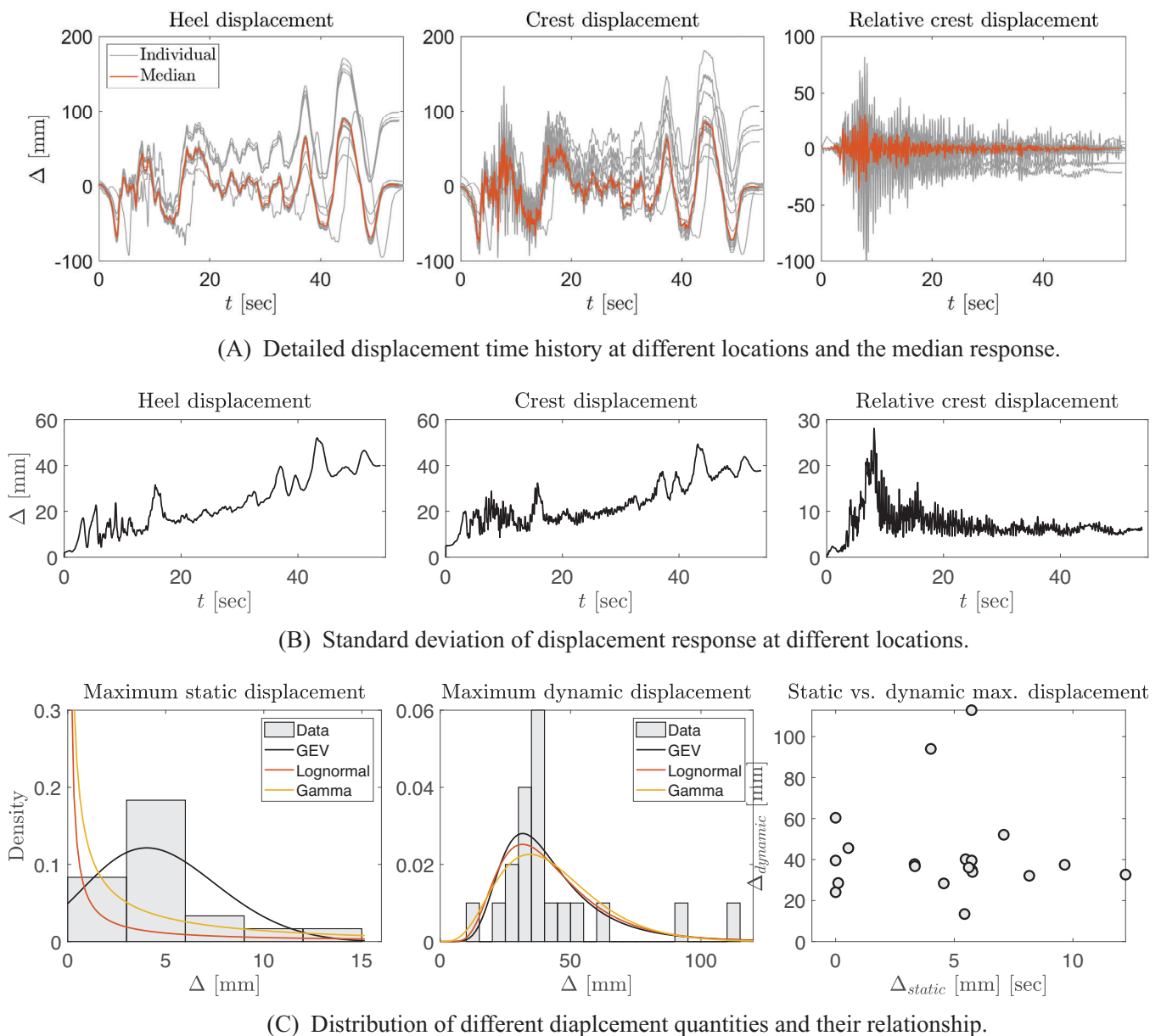


FIGURE 6 Processing displacement response under real ground motion record.

and absorption (including considerations for the free-field), choice of fluid element and approach for FSI, the selected concrete constitutive model and its response to dynamic loading-induced damage, the time integration scheme employed for stability control, and finally, the software package employed for analysis.

## 5.1 | Real ground motion

Figure 6 presents a summary of the results collected from 20 models, illustrating the displacement response. Prior to statistical analysis, all results underwent initial data filtering, and any outliers were subsequently removed. Individual displacement time histories for both the heel and crest, along with the relative crest displacement, are shown in Figure 6A. This figure also highlights the median values. The heel and crest displacements exhibit large oscillations, while the relative displacement demonstrates a high-frequency nature. Four models exhibit residual displacements at both the heel and crest points, which may indicate either relative sliding between the dam and the foundation block or a rigid body motion of the entire finite element model due to inadequate boundary conditions. This issue can often be resolved by introducing

a self-equilibrium loading condition, such as elastic boundary conditions, to one side of the foundation.<sup>1</sup> Among these four models, three employ viscous boundary conditions for the foundation, with one of them utilizing infinite elements. Additionally, one simulation exhibits a temporal shift and employs infinite elements for the foundation, including the rock-column and direct free field forces. In terms of the relative crest displacement history, two models exhibit residual displacement, both of which involve infinite elements. Notably, the most substantial relative crest displacement arises in a model utilizing a massless foundation approach with fixed boundary conditions. This case yields a maximum relative crest displacement approximately 2.5 times higher than the median value. This observation aligns with prior findings that distinguish between massed and massless foundation models.<sup>1</sup>

Figure 6B illustrates the standard deviation of displacement histories for both absolute and relative measurements. The absolute displacements at both the heel and crest locations exhibit a nearly linear increasing pattern, punctuated by intermittent spikes along this trajectory. Within the strong motion interval of the analysis (5–15 s), these displacements demonstrate standard deviations ranging from 10 to 30 mm. The highest standard deviation is approximately 50 mm, which can be compared to the previously mentioned median displacement of around 100 mm. In contrast, the pattern for the standard deviation of the relative crest displacement differs. Here, the maximum standard deviation occurs around 10 s (coinciding with the peak ground motion), followed by a decrease to a smaller and relatively stable value for the rest of the simulation.

All the previous comparisons have been conducted exclusively on “dynamic only” results, excluding the static response. Figure 6C provides a comprehensive overview of the maximum static and maximum dynamic displacement responses separately, along with three distributional models fitted to the data. The choice of using the generalized extreme value (GEV), lognormal, and gamma<sup>3</sup> distributions is arbitrary, as the goal here is not to determine the most suitable fit based on goodness-of-fit metrics. Given the limited scope of the database used in this study, any conclusion drawn from these models should not be regarded as definitive. As we will explore later in this section, with the exception of static displacement, these three models yield similar outcomes for all other cases. For maximum static displacement, the GEV model appears more reasonable, since the other two models result in very small mean or median values. Additionally, it is worth noting that the lognormal distribution is commonly employed in the fields of structural and earthquake engineering to describe the distribution of engineering demand parameters.<sup>105</sup>

For the maximum static displacement, the values vary from 0.2 mm to over 12 mm. The GEV model has a location value of 3.4 mm, which is close to the crude mean of 4.6 mm. Concerning the maximum dynamic displacement, values range from 13 to 112 mm, with a crude mean of 43 mm. All three distribution models exhibit striking similarity. The GEV model's  $\mu$  (location) value is 33 mm, while the lognormal model's median is 39 mm, and the logarithmic standard deviation is 0.45. This value coincides with the recommendations from EMA P695<sup>106</sup> regarding modeling uncertainty. EMA P695 characterizes modeling uncertainty through a matrix with two dimensions: (1) Representation of collapse characteristics and (2) Accuracy and robustness of models<sup>4</sup>. Each dimension encompasses three levels: high, medium, and low. For scenarios with a low representation of collapse and medium model accuracy (a condition that can be argued to apply in this study), a dispersion of 0.5 is recommended, which is analogous to the logarithmic standard deviation in the lognormal distribution. It is important to note that while this comparison is approximate, as FEMA P695 pertains directly to buildings and not concrete dams, there are similarities between them, as a concrete gravity dam functions as a cantilever-type short-period multi-degree-of-freedom system. They both share dynamic traits, responding to seismic forces through the transmission of loads at their bases. Additionally, their seismic behavior is influenced by the first few vibration modes.

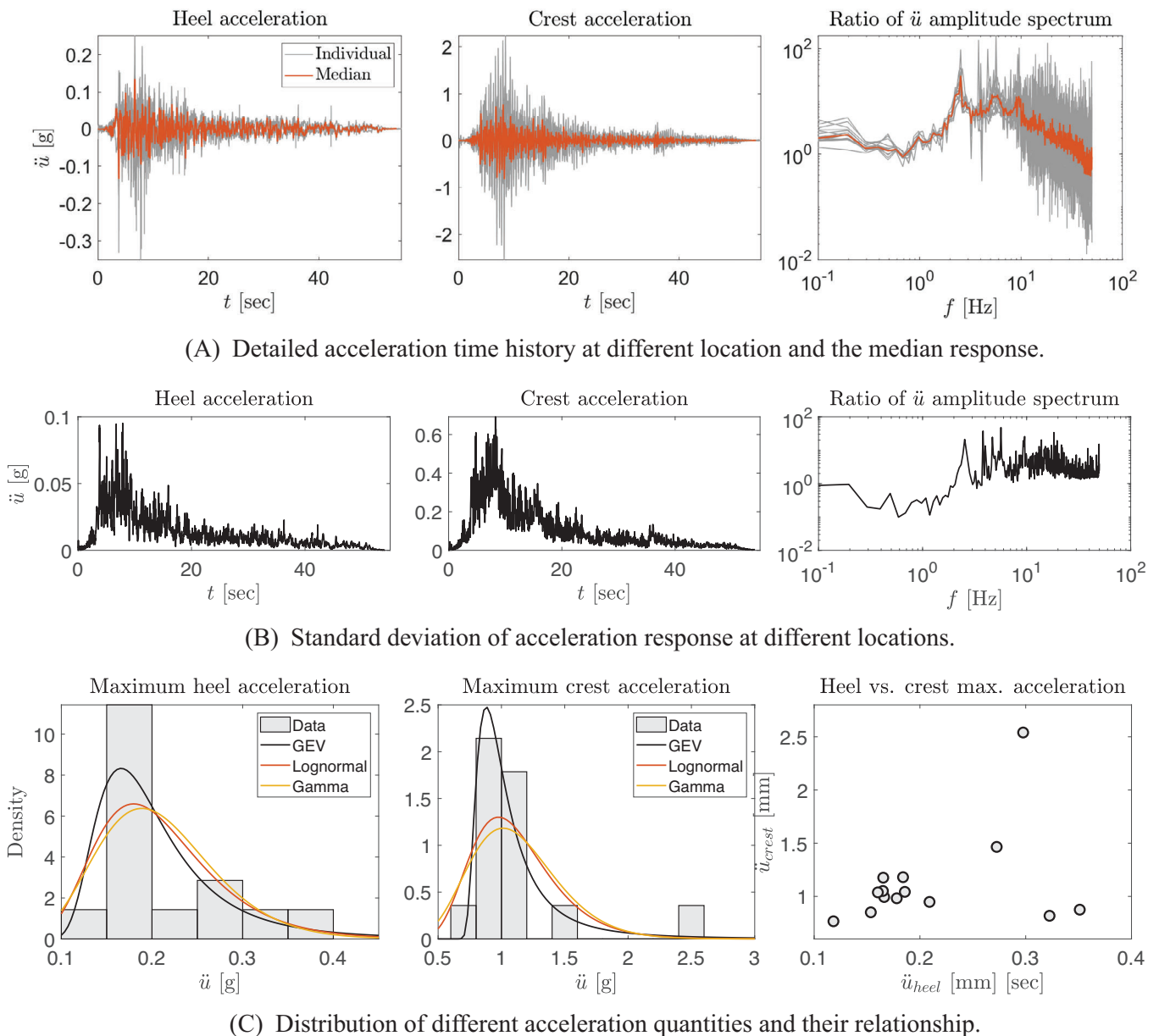
Lastly, Figure 6C (left) depicts the correlation between the maximum static and dynamic displacements. As seen, there is minimal correlation observed across different models. The static displacement is primarily influenced by hydrostatic pressure and the dam's self-weight, along with the stiffness of the foundation. It is worth mentioning that in certain instances, the hydrostatic pressure is applied solely to the dam, while in others, it is also applied to the upper face of the foundation.

Figure 7 employs a similar approach to the acceleration response analysis as discussed for displacement in Figure 6. Acceleration at the heel and crest points is depicted in Figure 7A (left and middle). Ideally, the acceleration at the heel should be similar or close to the free-surface Taft record displayed in Figure 5A. However, the median of the recorded heel

<sup>3</sup> The GEV model includes three parameters as shape, scale, and location factors. The lognormal model includes two parameters as log location and log scale. The gamma model includes two parameters as shape and scale factors.

<sup>4</sup> Representation of collapse characteristics refers to how completely and comprehensively the index archetype models capture the full range of design parameters and associated structural collapse behavior that is envisioned within the archetype design space. Accuracy and robustness of models refers to the degree to which nonlinear behaviors are directly simulated in the model, or otherwise accounted for in the assessment.





**FIGURE 7** Processing acceleration response under real ground motion record.

acceleration exhibits a smaller value. This discrepancy can be attributed to the modeling uncertainty in the foundation and its boundary conditions, including the free-field assumptions. As anticipated, the acceleration at the crest is amplified by approximately 10 times. To better represent the heel and crest acceleration time histories, they are presented as amplitude spectra in Figure 7A (right), showing the ratio of the acceleration amplitude spectrum. This ratio is obtained by computing the Fourier spectrum of the acceleration time series.

For frequencies below 1 Hz, the median response ratio is around 2. Between the frequency range of 5 to 10 Hz, the ratio fluctuates between 3 and 30, with an average value of 10. Beyond 10 Hz (up to about 50 Hz), the ratio gradually decays linearly to 0.5. Among the individual models, three show significant spikes, such as 170, in the amplitude spectrum ratio. Notably, all three models lack free-field boundary conditions.

The standard deviation of heel and crest acceleration time series follows a similar trend as displacement, peaking at the heel with a value of 0.1 g, equal to the median acceleration, Figure 7B. The standard deviation of acceleration spectrum amplitude averages around 0.8 for frequencies below 2 Hz, and then increases to an average value of 5 for  $f > 2$  Hz, accompanied by fluctuations.

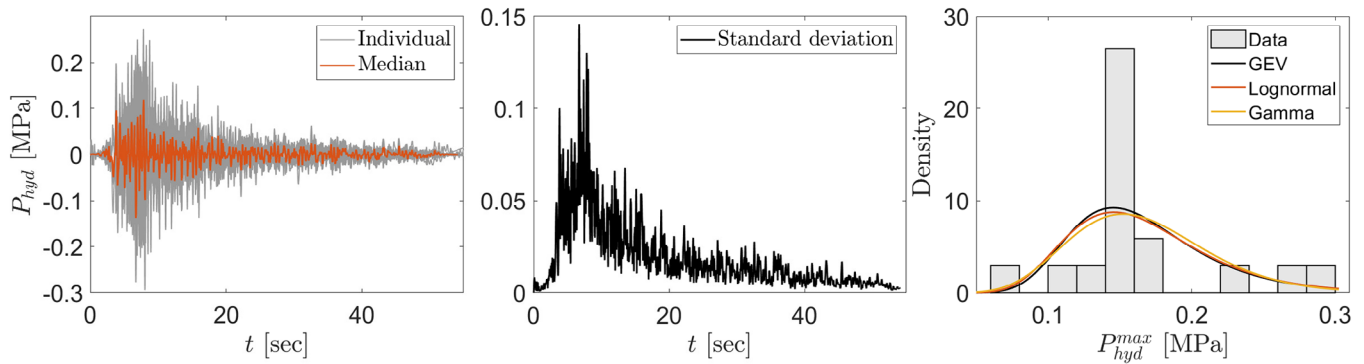


FIGURE 8 Processing hydrodynamic pressure response under real ground motion record.

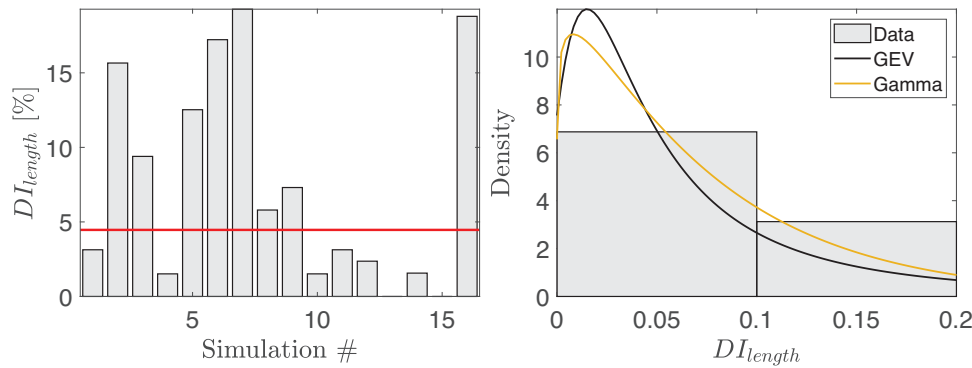


FIGURE 9 Processing DI under real ground motion record.

The fitted distributions for maximum (absolute) heel and crest accelerations are shown in Figure 7C (left and middle). The lognormal and gamma models show close agreement, while the GEV model exhibits a minor difference. Based on the lognormal distribution, the median values for maximum heel and crest accelerations are 0.2 and 1.07 g, respectively. The logarithmic standard deviation (dispersion) in both cases is approximately 0.3, which is lower than the displacement-based dispersion. Finally, Figure 7C (right) illustrates the relationship between maximum acceleration at the heel and crest. With the exception of two outliers, a positive correlation is evident. Further analysis of these two outliers indicates that both suffer from spikes in their heel acceleration responses, which can be attributed to numerical integration issues or the presence of superstructure (i.e., the dam) at the recording location.

Figure 8 employs a similar approach to analyze the hydrodynamic pressure,  $P_{hyd}$ , at the heel of the dam. Unlike the displacement response, no instances of residual or shifted values are observed for this parameter. The ratio of the maximum  $P_{hyd}$  to the median value is approximately 2. The trend in standard deviation is comparable to that observed for the relative crest displacement, with a peak value of around 0.15 MPa. It is noteworthy that the maximum  $P_{hyd}$  in the median response is even lower than 0.15 MPa. Lastly, Figure 7 (right) presents the distribution of the maximum  $P_{hyd}$ , which is consistent across the three distribution models. The lognormal model yields a median value of 0.16 MPa and a logarithmic standard deviation of 0.3, indicating less variation compared to the displacement response.

Figure 9 provides the DI for different simulations. Damage at the dam base (i.e., dam-foundation interface) is quantified as the ratio of cracked base length to the total base length,<sup>78</sup>  $DI = \frac{L_{cr}}{L_{tot}}$ . As seen in this figure, some simulations do not report any damage while some others report a damage as large as 18%. The median value from all simulations is about 4.5%. Five out of 16 simulations report DI of 10% or higher. Four of these models (including the two top ones) are all based on no free-field assumption for the foundation domain. Also, four of these models are associated with damage plasticity, and four simulations use implicit time integration scheme. Tracking the trends of models with no or small damage also reveals that they are different types of time integration scheme and concrete constitutive models; however, nearly all of them are based on free-field boundary condition. Therefore, the most influential modeling aspect in DI variation is foundation boundary condition and wave propagation assumption.

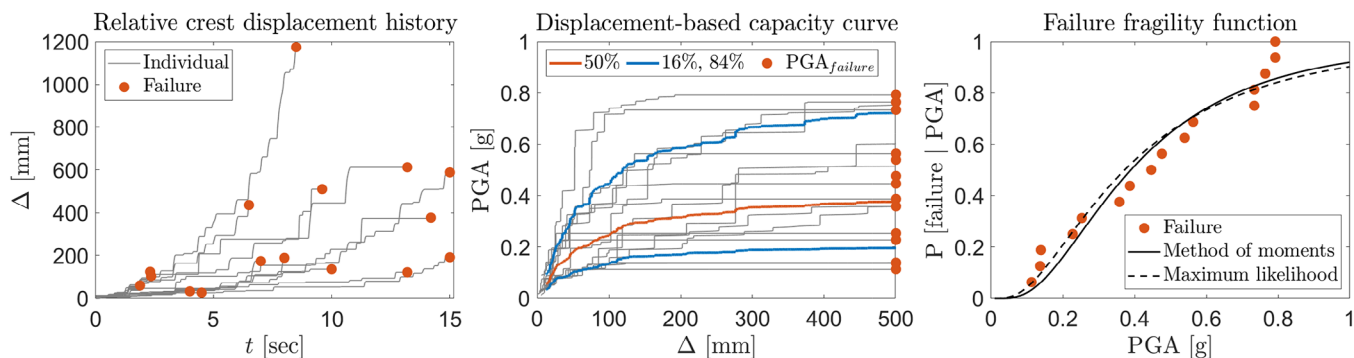


FIGURE 10 Processing displacement-based responses under IAA.

## 5.2 | Intensifying Artificial Acceleration

While conventional modeling UQ using a single real ground motion record is inherently limited by the specific attributes of that record, such as its frequency content and seismic intensity, the IAA offers a distinctive avenue for probing a broad spectrum of intensity levels without incurring additional computational costs. IAA further facilitates the comprehensive exploration of dam responses across varying seismic intensities in a continuous manner. In this context, 16 participants undertook analyses employing IAA. Similar response quantities as of the real ground motion were recorded.

Figure 10 (left) illustrates the temporal evolution of the maximum absolute relative crest displacement. In this plot, the displacement response terminated at the failure point. The determination of this failure time hinges on two primary criteria: (1) when the simulation reaches a juncture where certain engineering demand parameters surpass defined thresholds, for instance, when the DI at the base attains a value of one. Some participants used a displacement-based criteria, for example, 0.01% of dam height as failure criteria (other references propose 0.03%<sup>107</sup>). (2) when numerical instability emerges, triggering the automatic termination of the simulation due to unsatisfactory software internal criteria. Although the precision of establishing a failure point introduces an inherent uncertainty, it is important to acknowledge the absence of a universally accepted metric to quantitatively define failure (or collapse) in concrete dams. Notably, the U.S. Bureau of Reclamation's definition of structural failure as the uncontrolled release of reservoir water presents a qualitative description unamenable to integration within UQ efforts. As illustrated in Figure 10 (left), failure is observed to manifest at diverse levels of crest displacement and varied time intervals, ranging from 2 to 15 s, accompanied by failure displacements spanning 30 to 600 mm, with one notable instance reaching 1200 mm.

In IAA, the time parameter exhibits a direct correlation with seismic intensity. This relationship is explained by [78, 79], demonstrating the potential to convert the “time” parameter into different intensity measures, such as PGA or first-mode spectral acceleration. This study adopts the simplest approach: PGA is represented as  $PGA(t) \equiv \max\{\text{Abs}(\ddot{u}_g(\tau) : \tau \in [0, t])\}$ . Unlike the scalar nature of PGA in real ground motions, it is a time-dependent parameter within IAA application. Subsequently, the definition of displacement-based capacity curves ensues, depicting the relationship between displacement and PGA, as shown in Figure 10 (middle). Increasing PGA yields a nonlinear displacement response, ultimately leading to failure, as evidenced by the plateau in the capacity curve. Drawing inspiration from the IDA method,<sup>108</sup> the median, 16% and 84% fractiles are calculated for each individual capacity curve. The failure points are delineated by the right vertical line, allowing for the tracking of the failure PGA value,  $PGA_{failure}$ . It is paramount to reiterate that the variations observed in the individual capacity curves within Figure 10 (middle) are solely attributed to modeling uncertainty, devoid of any reflection of ground motion RTR variability, as dispelled by [109].

Leveraging the data obtained from failure capacity points, it is possible to construct an empirical CDF and fit various distributional models. In this study, it is assumed that these data points conform to a lognormal distribution, resulting in the development of a failure fragility-type function. Two distinct methodologies are employed: (1) Method of Moments (MM), which aligns the median and logarithmic standard deviation to match the moments of the data, and (2) Maximum Likelihood Estimation (MLE), which optimizes parameters to maximize a “likelihood” function based on either failed or safe data.<sup>110</sup> The comparison of these failure fragility functions is presented in Figure 10 (right). Notably, the MM and MLE methods exhibit remarkable closeness, yielding estimated medians of 0.39 and 0.37, and dispersions of 0.67 and 0.76, respectively. These dispersions surpass the RTR variability reported for the same concrete gravity dam, that is, 0.4.<sup>34</sup>

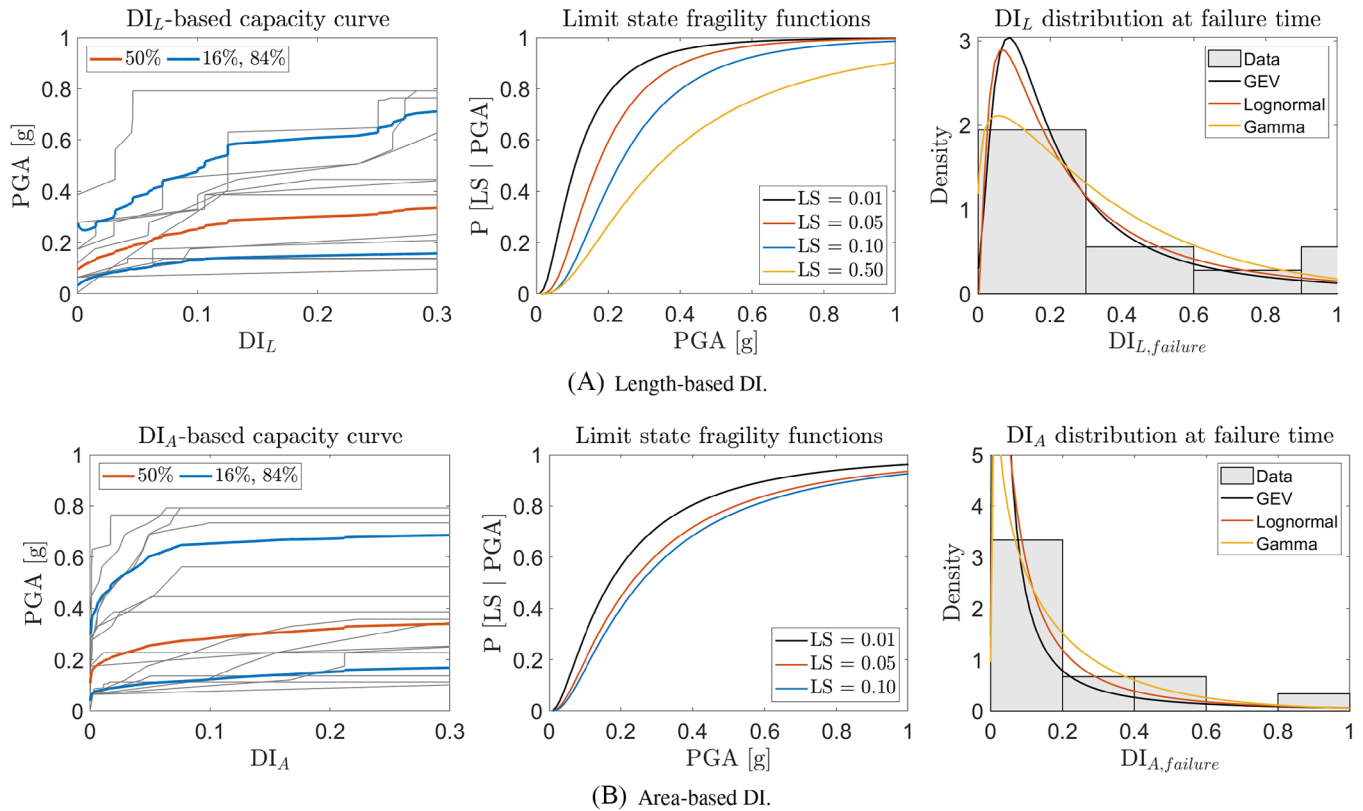


FIGURE 11 Processing damage indices under IAA.

Figure 11 illustrates capacity curves, fragility functions, and the distribution of the DI at the failure time, employing two different versions of the DI. The first one, the length-based DI discussed earlier, is complemented by the area-based DI. The area-based DI is quantified as the ratio of the cracked (cross-section) area to the total dam area, defined as  $DI = \frac{A_{cr}}{A_{tot}}$ . This global index offers an inclusive perspective of damage across various locations without a specific crack path. Figure A1 compares the evolution of DI based on these two definitions as computed by various participants. In some cases, the analysis is terminated at the failure time, while others continue to report the DI value for post-failure. Across all cases, it can be observed that the length-based damage index ( $DI_L$ ) consistently exceeds the area-based damage index ( $DI_A$ ) at any given time or equivalent intensity level. However, the specific ratio between the two indices varies based on the employed damage modeling techniques.

Figure 11A presents the length-based DI scenario, where the median failure PGA stands at 0.33 g. Four fragility functions are constructed corresponding to limit states (LS) of 1% (initiation), 5% (propagation), 10% (expansion), and 50% (critical) of the length-based DI. All functions are fitted using the MLE method. The medians for these four LS values progressively increase from 0.11, 0.17, 0.23 to 0.34 g, with dispersions varying at 0.8, 0.68, 0.67, and 0.83 respectively. These dispersion values slightly surpass those of the displacement-based fragility functions and can be attributed to concrete modeling complexities and the element size at the dam-foundation interface. Note that the crest displacement is a global response and is less sensitive to mesh size and other local effects. The fitted distributions for length-based damage indices using the GEV and lognormal distributions exhibit similarity, while the gamma distribution differs. The median of the lognormal distribution is 23%, signifying that half of the models encounter 23% of the base crack at the time of failure.

In Figure 11B, the median failure PGA is 0.34 g for area-based DI. Three fragility functions correspond to LSs of 1%, 5%, and 10% of the area-based DI. All three functions exhibit a similar dispersion of approximately 0.95, considerably larger than the displacement-based dispersion. Variability among results is exacerbated by the type of concrete constitutive model and mesh size. A larger mesh tends to create a more localized crack pattern, while a very fine mesh leads to diffusive (hair-like) crack propagation. The fitted distributions for area-based damage indices exhibit similarity, with the median of the lognormal distribution at 8.5%. This indicates that half of the models fail before reaching 8.5% of overall body damage.

Figure A2 presents the evolution of crack propagation and failure modes of the dam across different times in the IAA or equivalent PGA levels. In line with the variation observed in the DI and failure times, a substantial variability in crack

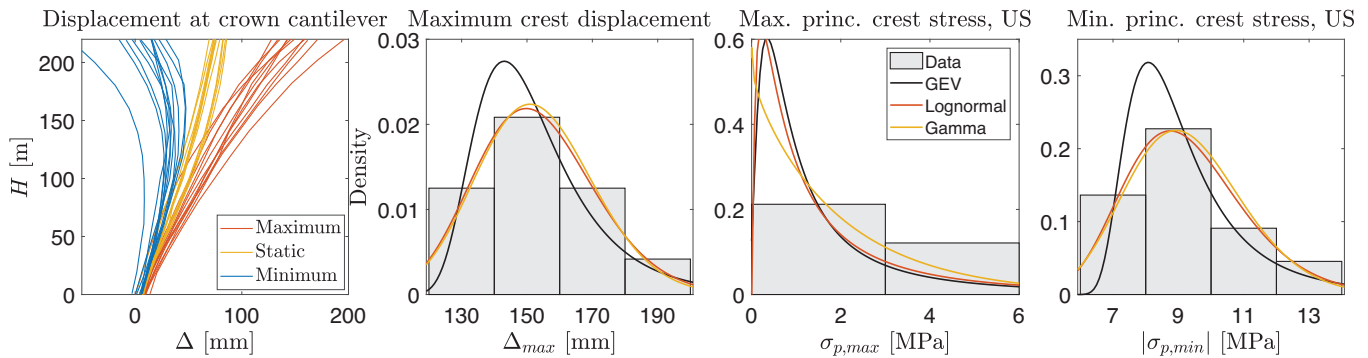


FIGURE 12 Processing modeling uncertainty results from the 12th ICOLD benchmark study.

propagation emerges, particularly concerning PGA (or time). The initiation of cracking is consistently observed at the heel point and near the downstream neck discontinuity across nearly all cases. The base crack progresses horizontally towards the dam's toe, while the inclined propagation of the crack at the neck heads upstream. Unlike the base crack, a noticeable pattern of multiple crack paths forms around the neck, with through cracks appearing before the base crack. Moreover, a series of crack paths develop along the downstream face, primarily at the mid-height of the dam, propagating downwards and towards the upstream face. Overall, the observed crack propagation in various cases aligns with findings from shake table tests on gravity dams.<sup>111–113</sup>

Among the models displayed in Figure A2, eight models (#31 and #33 excluded) adopt a free-field foundation boundary condition. However, specific conclusions regarding crack patterns based on foundation boundary conditions remain elusive. Notably, five of these models rely on Abaqus software and concrete damage plasticity (#16, #26, #28, #31, and #33). These models share a common FSI approach, albeit with variations in boundary conditions and mesh attributes. Despite similar crack profiles, they exhibit differences in the time (or equivalent PGA) when the crack patterns manifest. For example, the crack pattern observed at  $t = 3$  s (i.e., 0.17g) in model #16 is approximately replicated at  $t = 9$  (for #26),  $t = 5$  (for #28),  $t = 13$  (for #31), and  $t = 5$  (for #33).

Model #19 employs the Equivalent Linearization technique with large triangular elements (15 m), resulting in limited accuracy in predicting crack paths and associated DI values. Models #17 and #27, despite sharing similar foundation boundary conditions and concrete models, differ in their use of 2D plane strain and 3D slice model. While both models exhibit a similar trend in crack pattern and progression, the extent of damage at the dam's upper levels is greater in the 3D slice model, whereas the base crack at the dam-foundation interface is more pronounced in the 2D model.

## 6 | DISCUSSION

Other ICOLD benchmark workshops have also investigated various case studies with the objective of identifying best practices in seismic analysis of concrete dams. Notable examples include the 2013 workshop on seismic analysis of a symmetry arch dam, the 2015 workshop on an asymmetry arch dam, and the 2017 workshop on seismic analysis of an arch-gravity dam. This section aims to gather, refine, and quantify findings from these additional studies to facilitate meaningful comparisons with the outcomes presented in this paper.

### 6.1 | 12th ICOLD benchmark results

The 12th ICOLD benchmark<sup>114</sup> in 2013 revolved around a symmetric arch dam. Participants were provided with finite element meshes of the dam and foundation, as well as material properties, a three-component ground motion record, and suggested damping values. All simulations were conducted within the linear elastic analysis, without modeling any concrete damage or joints. The primary focus of this benchmark was to perform dynamic FSI analyses. The 12 participants submitted results, with 7 of them employing acoustic elements for fluid elements, while others adopted the added mass approach. Notably, most participants utilized massless foundation model rather than free-field boundary conditions. The collected data encompassed displacements and stresses at various locations. Figure 12 (left) visualizes the distribution of static and dynamic (maximum and minimum) displacements along the crown cantilever in the stream direction. Data points at the crest level were subjected to fitting with several distributional models. The computed dispersion value for displacement was notably small, at 0.12, which aligns with the linear nature of the simulations and the limited modeling



variability presented by FSI. This figure also shows the fitted distributions to the maximum and minimum principal stresses at the upstream point of the crest. It is important to note that this point was selected for uniformity of calculations, despite not necessarily representing the highest stress value. The computed dispersion attributed to stress was measured at 0.2.

## 6.2 | 13th ICOLD benchmark results

The 13th ICOLD benchmark<sup>115</sup> conducted in 2017 focused on an asymmetric arch dam. Participants were furnished with finite element meshes of the dam, foundation, reservoir information, material properties, three three-component ground motion records, and proposed damping values. The dynamic properties distinct from static ones. The benchmark also accounted for thermal gradients/analyses. While participants were advised to carry out linear simulations, the use of dam-foundation joints was permissible. Participants were tasked with providing displacement results along the crown cantilever, as well as the maximum and minimum principal stresses at 10 different locations: dam crest (left: A, center: B, and right: C), dam upper part (left: D, right: E), abutment upper (left: F and right: G), abutment lower (left: H, right: I), and dam lower part (J). Out of the total 11 participants, 5 of them employed compressible fluid elements in their analyses. Upon processing the crest displacement results, a dispersion value of 0.25 was computed. However, the benchmark's complexity introduced numerous uncontrolled modeling factors, rendering the generalization of results challenging and their reliability questionable.

Instead, Figure 13 illustrates the correlation matrix among the maximum principal stress values at 10 distinct locations. The diagonal cells depict the histogram of ranks for each location, incorporating a non-parametric kernel-smoothing distribution. Kernel distribution is employed due to the inability of a parametric distribution to adequately fit the data. The lower triangular cells exhibit the discrete rank values for any two locations, denoted as  $l_i$  and  $l_j$ , alongside their local regression using weighted linear least-squares and a 2nd-degree polynomial model. The upper triangular cells present the Spearman's linear correlation coefficient ( $R$ ) in the format of  $R = 1 - \frac{6 \sum d^2}{n(n^2-1)}$  (where  $d$  represents the difference between the ranks of the two columns, and  $n$  is the length of each column), along with  $p$ -values for assessing the hypothesis of no correlation against the alternative hypothesis of a nonzero correlation ( $P$ ). The correlation coefficient is further distinguished by a distribution of colors, spanning from  $-0.41$  (between locations D and F) to  $+0.93$  (between locations C and E). Consequently, excluding discussions of uncertainty in individual responses, this study highlights a substantial correlation between the points at the crest and upper parts. As the data processing progresses towards the abutment and lower part of the dam, the pattern and correlation of the results undergo notable changes (i.e., reduces in most cases).

## 6.3 | 14th ICOLD benchmark results

Finally, the 14th ICOLD benchmark study<sup>116</sup> has concentrated on the seismic analysis of an arch gravity dam. The provided finite element model of the dam encompasses its foundation, with options for both free-field and non-free-field boundary conditions. Concrete and rock material properties are provided, with the potential for nonlinearity being introduced through dam-foundation interface joints. However, the stiffness values for these joints are not specified. Various types of interface elements were employed, including frictional contact with a gap, cohesive law-based elements, spring elements, joint elements, node-to-surface contact, and surface-to-surface contact. The majority of simulations utilize an implicit time integration scheme. Depending on the complexity of the modeling, different coupled system problems are formulated. Foundation radiation boundary conditions encompass dashpot/Lysmer-Kuhlemeyer, perfectly matched layers, free-field, and node-to-surface contact with a penalty.

While several parameters were provided to participants, the presence of numerous modeling variables beyond direct control renders the UQ process challenging, particularly given the limited number of participants (ranging from 6 to 9 for different tasks). Three distinct seismic analyses are evaluated here, focusing on their relative variations rather than providing generalized recommended values for future studies: Mod-I involves linear time-history analysis with simplified dynamic interactions (massless foundation), with the recommended use of generalized Westergaard's added masses. Mod-II entails nonlinear time-history analysis (applying uplift as external forces and allowing the interface elements to model opening) with simplified dynamic interactions. Mod-III centers around linear time-history analysis with advanced dynamic interactions (utilizing dynamic FSI and free-field foundation boundary conditions).

According to Figure 14, it becomes evident that utilizing Mod-III (linear analysis with advanced interaction models) reduces the median and dispersion of the displacement response in comparison to Mod-I (linear analysis with simplified

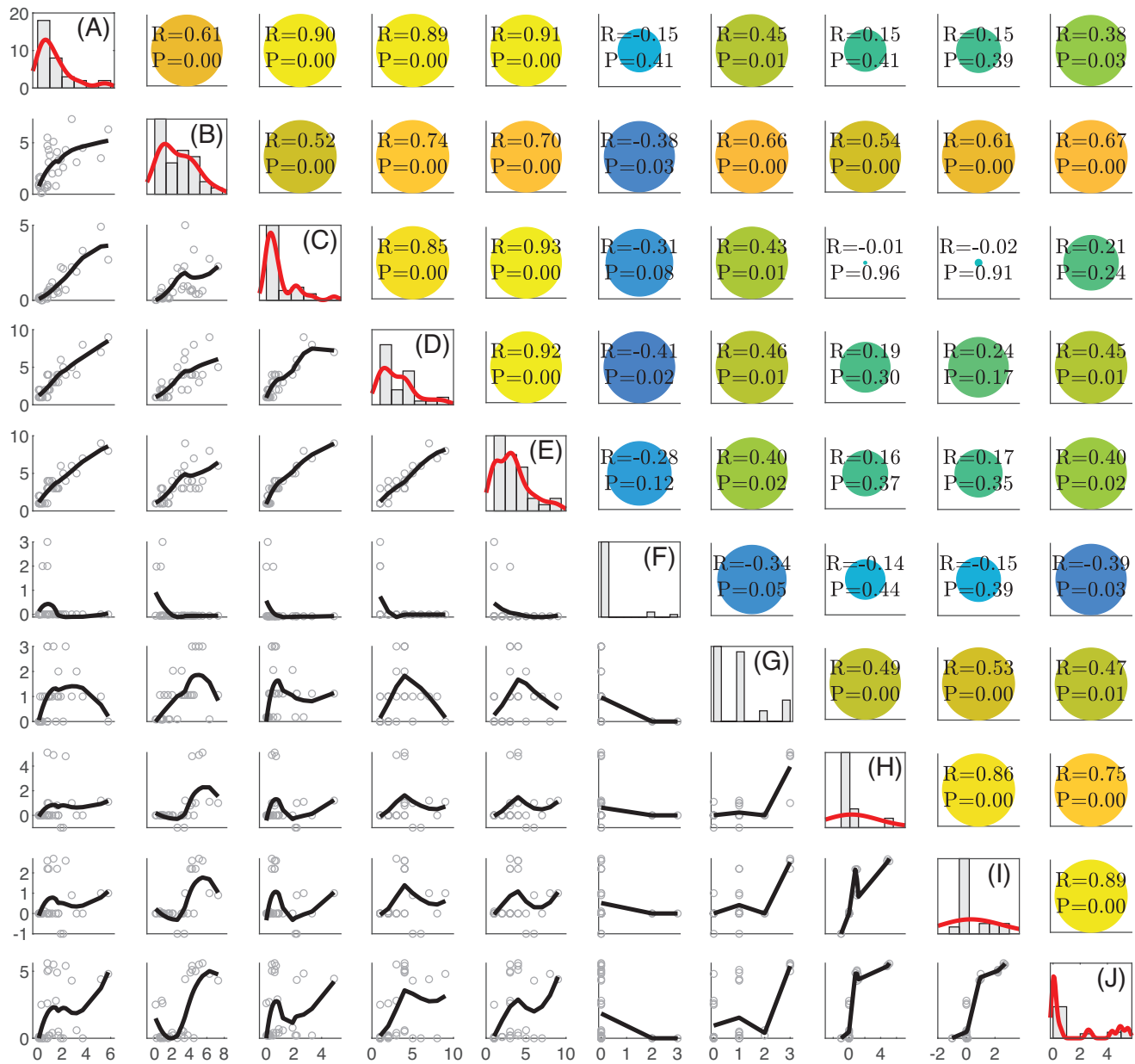


**FIGURE 13** Correlation among maximum principal stress values at 10 different locations collected from outcome collected from the 13th ICOLD benchmark study.

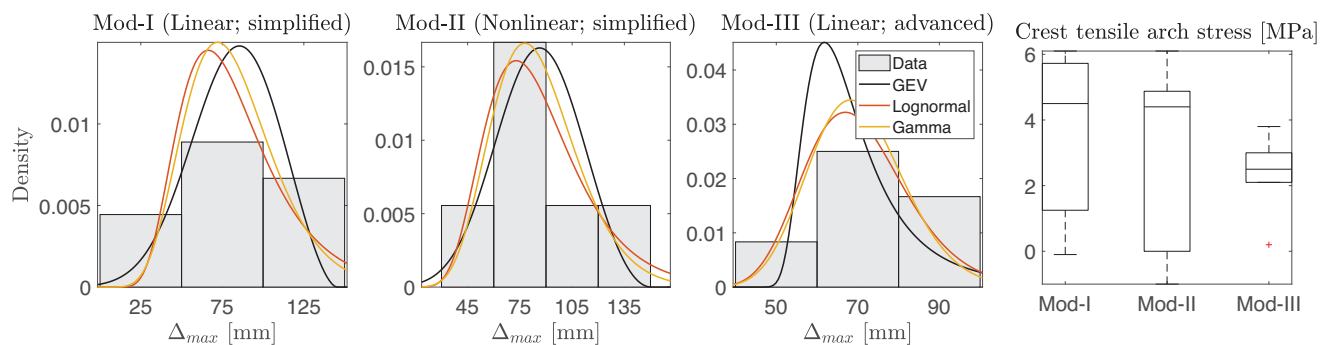


**FIGURE 14** Processing modeling uncertainty results from the 14th ICOLD benchmark study.

interaction). Therefore, a bias term can be identified in simplified model compared to the advanced one. The employment of the nonlinear model (Mod-II) increases the median displacement in comparison to the linear model (Mod-I), but it does not significantly impact the dispersion value. The logarithmic standard deviation (i.e., dispersion) for the three model types (I, II, III) is measured at 0.39, 0.37, and 0.18, respectively. This figure also visualizes the results of tensile arch stresses at the crest in the form of box-plots. The utilization of advanced interaction models (Mod-III) leads to a reduction in dam stresses. Hence, it is apparent that the accurate modeling of the foundation-dam-reservoir coupled system, particularly with respect to the interface joint, takes precedence. These results are pertinent to the specific ground motion record provided for the study.

## 7 | CONCLUSIONS, RECOMMENDATIONS, AND FUTURE WORK

Our comparative analysis, spanning a range of benchmark cases, emphasized the substantial impact of modeling-related uncertainties on key dam response parameters: displacement, DI, stress distribution, crack propagation, and failure modes. These modeling variations encompass factors such as mesh type, mesh size, time step used in numerical simulation, convergence criteria, foundation model and associated boundary conditions for wave propagation and absorption, fluid element selection and FSI approach, chosen concrete constitutive model and its damage response, time integration scheme for stability control, and the software package for analysis.

### 7.1 | Concluding remarks

Using various distributional models, including the lognormal, GEV, and gamma models, we have furthered our understanding. Notably, the lognormal distribution has allowed us to quantify the logarithmic standard deviation, referred to as dispersion ( $\beta_{mod}$ ). Its importance arises from its potential integration with other sources of uncertainty, such as ground motion RTR variability ( $\beta_{RTR}$ ) and material randomness ( $\beta_{mat}$ ), via SRSS combination.

By examining the dam response under the influence of a single component of the Taft ground motion record with a PGA of 0.18 g, the following high-level conclusions can be drawn. The computed  $\beta_{mod}$  (assuming a lognormal distribution) is found to be 0.45, 0.30, 0.32, and 0.30 for the maximum dynamic crest displacement, maximum hydrodynamic pressure at the heel, heel and crest maximum acceleration, respectively. The time-dependent standard deviation values exhibit a nearly linear increasing pattern, occasionally punctuated by intermittent spikes along this trajectory. Conversely, the pattern for the standard deviation of the relative crest displacement, absolute heel and crest acceleration, and heel hydrodynamic pressure differs. In this context, the maximum standard deviation is observed around 5–10 s, corresponding to the strong motion part of the applied record, followed by a decrease to a smaller and relatively stable value for the remainder of the simulation. The length-based DI results spanned from 0%–18%, with a median of 4.5%. Detailed discussions on the contributions of different modeling uncertainties and assumptions are presented in the paper and are not reiterated here.

On the other hand, the IAA approach provided a unique opportunity to investigate the progression of failure in concrete dams under various modeling strategies. This methodology has yielded a series of intensity-dependent capacity functions for displacement and DI. Moreover, we introduced a novel fragility function that primarily reflects level III and IV modeling variability. At the time of failure, the dispersion of  $PGA_{failure}$  was computed to be approximately 0.7, surpassing the typical ground motion RTR validity of 0.4, highlighting the significance of modeling uncertainty in the failure analysis of dams. Depending on the assumed limit state value, the dispersion of the DI may vary within the range of 0.67–0.83 for the length-based criterion and around 0.95 for the area-based criterion. Such pronounced dispersion results from the low level of confidence in damage analysis of concrete dams and the accurate documentation of the DI.

### 7.2 | Recommendations

Based on the results of the four ICOLD benchmark studies examined in this paper (one in-depth and three discussed), coupled with insights from published materials on numerical simulations of concrete dams,<sup>1,117</sup> several general recommendations are proposed to foster confidence and credibility in modeling and computational simulations.

The incorporation of fluid-structure dynamic interaction is important for accurate hydrodynamic pressure determination on the dam's upstream face. The utilization of compressible fluid elements is advised for advanced analyses. Utilizing simplified models may inadequately replicate the actual hydrodynamic pressure acting on the dam face, particularly in the presence of complex geometries and multi-component seismic excitation.

The dynamic interaction between the foundation and dam significantly influences safety assessment and potential failure modes, particularly in the context of severe seismic scenarios. It is imperative to establish non-reflecting boundary conditions for the foundation block to mitigate any manifestation of unrealistic response. Emphasizing the utilization of free-field boundary conditions takes precedence, surpassing other considerations like system nonlinearity. This strategic preference is grounded in recognizing the macro-scale impact of dam-foundation interaction across a broad spectrum of seismic intensities, wherein system nonlinearity assumes a more micro-level significance, predominantly manifesting at high seismic intensity levels.

In scenarios involving high seismic loading, introducing nonlinearity into the coupled system is imperative. Cohesive crack models, capable of accounting for crack opening, closing, and sliding, should be employed at known crack or joint locations. However, if the location of these features is not known beforehand, a continuum crack model should be applied to the entire dam, allowing cracks to evolve based on the external load. Through a sequence of iterative simulations, discrete cracks can subsequently replace smeared cracks at specific locations, providing a more direct control over the nature of potential joint sliding and openings. It is also recommended to avoid a mixture of linear elastic and nonlinear regions within the system. This can distort stress distribution and lead to unrealistic responses at the linear-nonlinear interface.

Factors such as mesh type and size, time step, convergence criteria, time integration scheme for stability control, damping model, and critical damping value all exert influence in seismic analyses of concrete dams, especially in the nonlinear phase. The use of implicit schemes is favored for nonlinear analyses, despite their computational demands. Aspects such as the dam's stage construction, gradual reservoir impoundment, thermal stresses (especially in 3D models), and the reservoir bottom wave reflection coefficient can impact initial stress states and structural results.

### 7.3 | Limitations and future work

In this study, we explored modeling-related uncertainties in seismic analysis of concrete dams, examining a diverse range of dam types and modeling approaches through ICOLD benchmark workshops. The variations in responses from different modeling strategies underscore the complex interplay between choices and predictions, emphasizing the need for accurate representation in dam behavior under seismic loads.

**Limitations:** Our study, while comprehensive, has some limitations. The assumed homogeneity in dam and foundation materials might not fully capture the heterogeneity present, especially in older dams. Non-homogeneous foundations with varying layer thicknesses pose challenges in wave propagation and deconvolution. For long canyon dams, spatial variability in ground motions requires consideration for wave passage and incoherency. Seismic responses to multi-component ground motion differ from single-component motion, and the characteristics of input ground motion, such as long-duration or near-fault motion, directly influence structural responses.

**Future Work:** Reducing modeling uncertainties necessitates a robust validation and verification process for finite element simulations. Future endeavors should concentrate on formulating a comprehensive roadmap for conducting structural analysis of concrete dams, incorporating a rigorous verification and validation framework. This effort should be complemented by extensive laboratory experiments and field measurements. The verification process must encompass code verification, solution verification, and the distinction between numerical errors and uncertainties. It is crucial to emphasize that validation should always follow verification to mitigate the accumulation of errors within computational models.

**Practical Implications:** The study's outcomes carry practical implications for seismic analysis in dam engineering. Our quantification of modeling uncertainties underscores the need for rigorous practices and parameter selection to ensure reliable outcomes. Engineers and practitioners should prioritize validation and verification in finite element simulations, considering the complexities introduced by modeling, materials and ground motion characteristics.

### ACKNOWLEDGMENTS

The author acknowledges the contributions of Dr Jerzy Salamon (US Bureau of Reclamation), Dr Richard Malm (formerly in KTH Royal Institute of Technology), and Ms Giorgia Faggiani (Ricerca Sistema Energetico) in formulating the ICOLD benchmark problem. Gratitude is also extended to all workshop participants whose invaluable insights and contributions have greatly enriched our understanding of modeling variability in seismic analysis of concrete dams. The author extends gratitude to Dr Siamak Sattar (National Institute of Standards and Technology) for general discussion on modeling uncertainty quantification, and benchmark data processing. The presented materials and conclusions in this paper solely represent the author's studies and opinions and do not reflect the views or opinions of others in any way.

## CONFLICT OF INTEREST STATEMENT

The author declares no potential conflict of interests.

## DATA AVAILABILITY STATEMENT

The data that support the findings of this study are available from the corresponding author upon reasonable request.

## REFERENCES

1. Saouma VE, Hariri-Ardebili MA. *Aging, Shaking, and Cracking of Infrastructures: From Mechanics to Concrete Dams and Nuclear Structures*. Springer; 2021.
2. Roache PJ. *Verification and Validation in Computational Science and Engineering*. Vol 895. Hermosa Albuquerque; 1998.
3. Roy CJ, Oberkampf WL. A comprehensive framework for verification, validation, and uncertainty quantification in scientific computing. *Comput Meth Appl Mech Eng*. 2011;200(25-28):2131-2144.
4. Ewing ME, Liechty BC, Black DL. A general methodology for uncertainty quantification in engineering analyses using a credible probability box. *J Verif Valid Uncertain Quantif*. 2018;3(2):021003.
5. Ayyub BM, Chao R. Uncertainty modeling in civil engineering with structural and reliability applications. *Uncertainty modeling and analysis in civil engineering*. CRC Press; 1998:1-8.
6. Bukenya P, Moyo P, Beushausen H, Oosthuizen C. Health monitoring of concrete dams: a literature review. *J Civ Struct Health Monit*. 2014;4(4):235-244.
7. Alves S, Hall J. System identification of a concrete arch dam and calibration of its finite element model. *Earthquake Eng Struct Dyn*. 2006;35(11):1321-1337.
8. Harris DW, Snorteland N, Dolen T, Travers F. Shaking table 2-D models of a concrete gravity dam. *Earthquake Eng Struct Dyn*. 2000;29(6):769-787.
9. Uchita Y, Shimpo T, Saouma V. Dynamic centrifuge tests of concrete dams. *Earthquake Eng Struct Dyn*. 2005;34:1467-1487.
10. Bolzon G, Sterpi D, Mazzà G, Frigerio A. *Numerical Analysis of Dams: Proceedings of the 15th ICOLD International Benchmark Workshop*. Vol 91. Springer Nature; 2020.
11. Salamon J. *Evaluation of Numerical Models and Input Parameters in the Analysis of Concrete Dams*. Tech. Rep. DSO-19-13. US Bureau of Reclamation; 2018.
12. Hariri-Ardebili MA, Seyed-Kolbadi S, Kianoush M. FEM-based parametric analysis of a typical gravity dam considering input excitation mechanism. *Soil Dyn Earthquake Eng*. 2016;84:22-43.
13. Sevieri G. *The Seismic Assessment of Existing Concrete Gravity Dams: FE Model Uncertainty Quantification and Reduction*. PhD thesis. University of Braunschweig and University of Florence; 2019.
14. Poul MK. *Development of Viscoelastic PML and Deconvolution of Input Motion at Depth for Soil-Structure Interaction—Application to Dams*. PhD thesis. Drexel University; 2019.
15. Jalayer F, Iervolino I, Manfredi G. Structural modeling uncertainties and their influence on seismic assessment of existing RC structures. *Struct Saf*. 2010;32(3):220-228.
16. Gokkaya BU, Baker JW, Deierlein GG. Quantifying the impacts of modeling uncertainties on the seismic drift demands and collapse risk of buildings with implications on seismic design checks. *Earthquake Eng Struct Dyn*. 2016;45(10):1661-1683.
17. Haindl M, Burton H, Sattar S. Quantification of equivalent strut modeling uncertainty and its effects on the seismic performance of masonry infilled reinforced concrete frames. *J Earthquake Eng*. 2023:1-21.
18. Li H, Li L, Zhou G, Xu L. Effects of various modeling uncertainty parameters on the seismic response and seismic fragility estimates of the aging highway bridges. *Bull Earthquake Eng*. 2020;18:6337-6373.
19. O'Reilly GJ, Sullivan TJ. Quantification of modelling uncertainty in existing Italian RC frames. *Earthquake Eng Struct Dyn*. 2018;47(4):1054-1074.
20. Sattar S, Liel AB, Martinelli P. *Quantification of Modeling Uncertainties Based on the Blind Prediction Contest Submissions*. ASCE; 2013:1997-2008.
21. Parisse F, Cattari S, Marques R, et al. Benchmarking the seismic assessment of unreinforced masonry buildings from a blind prediction test. *Structures*. 2021;31:982-1005.
22. Tomić I, Penna A, DeJong M, et al. Shake-table testing of a stone masonry building aggregate: overview of blind prediction study. *Bull Earthquake Eng*. 2023:1-43.
23. Vassiliou MF, Broccardo M, Cengiz C, et al. Shake table testing of a rocking podium: Results of a blind prediction contest. *Earthquake Eng Struct Dyn*. 2021;50(4):1043-1062.
24. Folz B, Filiatrault A. Blind predictions of the seismic response of a woodframe house: an international benchmark study. *Earthq spectra*. 2004;20(3):825-851.
25. Bartoli G, Betti M, Biagini P, et al. Epistemic uncertainties in structural modeling: a blind benchmark for seismic assessment of slender masonry towers. *Bull Earthquake Eng*. 2017;31(5):04017067.
26. Winkler RL. Uncertainty in probabilistic risk assessment. *Reliab Eng Syst Saf*. 1996;54(2-3):127-132.
27. Ellingwood B. Issues related to structural aging in probabilistic risk assessment of nuclear power plants. *Reliab Eng Syst Saf*. 1998;62(3):171-183.



28. Parry GW. The characterization of uncertainty in probabilistic risk assessments of complex systems. *Reliab Eng Syst Saf*. 1996;54(2-3):119-126.
29. Helton JC, Johnson JD, Oberkampf WL, Sallaberry CJ. Representation of analysis results involving aleatory and epistemic uncertainty. *Int J Gen Syst*. 2010;39(6):605-646.
30. Ang AHS. *Extended Reliability Basis of Structural Design Under Uncertainties*. Tech. Rep., SAE Technical Paper; 1970.
31. Der-Kiureghian A, Ditlevsen O. Aleatory or epistemic? Does it matter? *Struct Saf*. 2009;31:105-112.
32. Ang AHS, Tang WH. *Probability Concepts in Engineering Planning and Design: Emphasis on Application to Civil and Environmental Engineering*. Wiley; 2007.
33. Melchers RE, Beck AT. *Structural reliability analysis and prediction*. John Wiley & sons; 2018.
34. Hariri-Ardebili MA, Saouma V. Collapse Fragility Curves for Concrete Dams: Comprehensive Study. *J Struct Eng*. 2016;142(10):04016075.
35. Soysal B, Binici B, Arici Y. Investigation of the relationship of seismic intensity measures and the accumulation of damage on concrete gravity dams using incremental dynamic analysis. *Earthquake Eng Struct Dyn*. 2016;45:719-737.
36. Alembagheri M, Ghaemian M. Seismic assessment of concrete gravity dams using capacity estimation and damage indexes. *Earthquake Eng Struct Dyn*. 2013;42:123-144.
37. Segura R, Bernier C, Monteiro R, Paultre P. On the seismic fragility assessment of concrete gravity dams in eastern Canada. *Earthq spectra*. 2019;35(1):211-231.
38. Segura R, Padgett JE, Paultre P. Metamodel-based seismic fragility analysis of concrete gravity dams. *J Struct Eng*. 2020;146(7):04020121.
39. Hariri-Ardebili MA, Saouma V, Porter K. Quantification of seismic potential failure modes in concrete dams. *Earthquake Eng Struct Dyn*. 2016;45:979-997.
40. Hariri-Ardebili MA, Saouma V. Probabilistic seismic demand model and optimal intensity measure for concrete dams. *Struct Saf*. 2016;59:67-85.
41. Yazdani Y, Alembagheri M. Seismic vulnerability of gravity dams in near-fault areas. *Soil Dyn Earthquake Eng*. 2017;102:15-24.
42. Gorai S, Maity D. Seismic fragility assessment of concrete gravity dams under near source synthetic ground motions. *Struct Infrastruct Eng*. 2023:1-21.
43. Tidke AR, Adhikary S. Optimal intensity measure selection and probabilistic seismic demand models for dam-reservoir-layered foundation system. *Structures*. 2022;37:318-337.
44. Hariri-Ardebili MA, Chen S, Mahdavi G. Machine learning-aided PSDM for dams with stochastic ground motions. *Adv Eng Inf*. 2022;52:101615.
45. Hariri-Ardebili MA, Saouma V. Seismic fragility analysis of concrete dams: a state-of-the-art review. *Eng Struct*. 2016;128:374-399.
46. Sevieri G, De Falco A, Andreini M, Matthies HG. Hierarchical Bayesian framework for uncertainty reduction in the seismic fragility analysis of concrete gravity dams. *Eng Struct*. 2021;246:113001.
47. Hariri-Ardebili MA. Uncertainty quantification of heterogeneous mass concrete in macro-scale. *Soil Dyn Earthquake Eng*. 2020;137:106137.
48. Bradley BA. A framework for validation of seismic response analyses using seismometer array recordings. *Soil Dyn Earthquake Eng*. 2011;31(3):512-520.
49. Bradley BA. A critical examination of seismic response uncertainty analysis in earthquake engineering. *Earthquake Eng Struct Dyn*. 2013;42(11):1717-1729.
50. Chryssanthopoulos MK, Dymiotis C, Kappos AJ. Probabilistic evaluation of behaviour factors in EC8-designed R/C frames. *Eng Struct*. 2000;22(8):1028-1041.
51. Ibarra LF, Krawinkler H. *Global Collapse of Frame Structures under Seismic Excitations*. Pacific Earthquake Engineering Research Center Berkeley; 2005.
52. Lee T, Mosalam K. *Probabilistic Seismic Evaluation of Reinforced Concrete Structural Components and Systems*. Tech. Rep. 2006/04. Pacific Earthquake Engineering Research Center; 2006.
53. Haselton C, Deierlein G. *Assessing Seismic Collapse Safety of Modern Reinforced Concrete Moment Frame Buildings*. Report No. Tech. Rep., TR 156. John A. Blume Earthquake Engineering Center Department of Civil Engineering; 2006.
54. Aslani H, Miranda E. *Probabilistic Earthquake Loss Estimation and Loss Disaggregation in Buildings*. PhD thesis. Stanford University; 2005.
55. Browning J, Li YR, Lynn A, Moehle JP. Performance assessment for a reinforced concrete frame building. *Earthq spectra*. 2000;16(3):541-555.
56. Willam K, Pramono E, Stur S. Fundamental issues of smeared crack models. In: *Fracture of Concrete and Rock: SEM-RILEM International Conference June 17-19*. Houston, Texas, USA; 1987:192-207.
57. Jirásek M, Bazant ZP. *Inelastic Analysis of Structures*. John Wiley & sons; 2001.
58. Bittnar Z, Šejnoha J. *Numerical Methods in Structural Mechanics*. ASCE Press and Thomas Telford; 1996.
59. Bažant ZP, Planas J. *Fracture and Size Effect in Concrete and other Quasibrittle Materials*. Routledge; 2019.
60. Bybordiiani M, Arici Y. The use of 3D modeling for the prediction of the seismic demands on the gravity dams. *Earthquake Eng Struct Dyn*. 2017;46(11):1769-1789.
61. Lallemant D, Kiremidjian A, Burton H. Statistical procedures for developing earthquake damage fragility curves. *Earthquake Eng Struct Dyn*. 2015;44:1373-1389.
62. Cornell CA, Jalayer F, Hamburger RO, Foutch DA. Probabilistic basis for 2000 SAC federal emergency management agency steel moment frame guidelines. *J Struct Eng*. 2002;128(4):526-533.
63. Zareian F, Krawinkler H. Assessment of probability of collapse and design for collapse safety. *Earthquake Eng Struct Dyn*. 2007;36(13):1901-1914.

64. Hariri-Ardebili MA, Saouma V. Sensitivity and uncertainty quantification of the cohesive crack model. *Eng Fract Mech.* 2016;155:18-35.
65. Rea D, Liaw C, Chopra AK. *Dynamic properties of pine flat dam.* Tech. Rep., California Univ Berkeley Earthquake Engineering Research Center; 1972.
66. Chopra AK, Chakrabarti P, Gupta S. *Earthquake Response of Concrete Gravity Dams Including Hydrodynamic and Foundation Interaction Effects.* Tech. Rep., California Univ Berkeley Earthquake Engineering Research Center; 1980.
67. Fenves G, Chopra A. *Simplified Analysis for Earthquake Resistant Design of Concrete Gravity Dams.* Tech. Rep. UCB/EERC-85/10. Earthquake Engineering Research Center; 1986.
68. Fenves G, Chopra A. *EAGD-84: A Computer Program for Earthquake Analysis of Concrete Gravity Dams.* University of California, Earthquake Engineering Research Center; 1984.
69. Chavez JW, Fenves GL. *Earthquake Analysis and Response of Concrete Gravity Dams Including Base Sliding.* Earthquake Engineering Research Center, University of California; 1993.
70. Chávez JW, Fenves G. Earthquake response of concrete gravity dams including base sliding. *J Struct Eng.* 1995;121(5):865-875.
71. Chávez JW, Fenves GL. Earthquake analysis of concrete gravity dams including base sliding. *Earthquake Eng Struct Dyn.* 1995;24(5):673-686.
72. Salamon J, Wood C, Hariri-Ardebili MA, Malm R, Faggiani G. *Seismic Analysis of Pine Flat Concrete Dam: Formulation and Synthesis of Results.* Springer; 2019:3-97.
73. Løkke A. *Direct Finite Element Method for Nonlinear Earthquake Analysis of Concrete Dams Including Dam-Water-Foundation Rock Interaction.* PhD thesis. Norwegian University of Science and Technology; 2018.
74. Bhattacharjee S, Leger P. Seismic cracking and energy dissipation in concrete gravity dams. *Earthquake Eng Struct Dyn.* 1993;22(11):991-1007.
75. Fenves G, Chopra AK. Effects of reservoir bottom absorption and dam-water-foundation rock interaction on frequency response functions for concrete gravity dams. *Earthquake Eng Struct Dyn.* 1985;13(1):13-31.
76. Poul MK, Zerva A. Nonlinear dynamic response of concrete gravity dams considering the deconvolution process. *Soil Dyn Earthquake Eng.* 2018;109:324-338.
77. Poul MK, Zerva A. Efficient time-domain deconvolution of seismic ground motions using the equivalent-linear method for soil-structure interaction analyses. *Soil Dyn Earthquake Eng.* 2018;112:138-151.
78. Hariri-Ardebili MA, Saouma V. Quantitative failure metric for gravity dams. *Earthquake Eng Struct Dyn.* 2015;44:461-480.
79. Hariri-Ardebili MA, Furgani L, Meghella M, Saouma V. A new class of seismic damage and performance indices for arch dams via ETA method. *Eng Struct.* 2016;110:145-160.
80. Liang C, Chen J, Xu Q, Li J. Correlation study between seismic intensity measures and nonlinear response of arch dam via endurance time analysis. *KSCE J Civ Eng.* 2021;25(1):256-271.
81. Xu Q, Xu S, Chen J, Li J. A Modified Endurance Time Analysis Algorithm to Correct Duration Effects for a Concrete Gravity Dam. *Int J Geomech.* 2022;22(2):04021285.
82. Xu Q, Zhang T, Chen J, Li J, Xu S. A new endurance time analysis method for damage evaluation of high arch dams under the oblique incidence of mainshock-aftershock seismic sequences by wavelet decomposition. *Soil Dyn Earthquake Eng.* 2022;161:107406.
83. Alegre A, Oliveira S, Mendes P, Proença J, Ramos R, Carvalho E. Seismic safety assessment of arch dams using an ETA-based method with control of tensile and compressive damage. *Water.* 2022;14(23):3835.
84. Salamon J, Hariri-Ardebili MA, Estekanchi H, Mashayekhi M. *Seismic Assessment of a Dam-Foundation-Reservoir System Using Endurance Time Analysis.* CRC Press; 2019:2649-2659.
85. Hariri-Ardebili MA, Sattar S. Uncertainty and bias in fragility estimates by intensifying artificial accelerations. *Probab Eng Mech.* 2023:103545.
86. Enzell J, Malm R, Abbasiverki R, Ahmed L. *Non-linear Behavior of a Concrete Gravity Dam During Seismic Excitation: A Case Study of the Pine Flat Dam.* Springer; 2021:99-112.
87. Faggiani G, Masarati P, Frigerio A. *Assessment of the Dynamic Response of Pine Flat Concrete Gravity Dam. FEM Simulation of Dam-Foundation Interaction.* Springer; 2021:113-127.
88. Farrokh M. *Seismic Analysis and Damage Evaluation of Pine Flat Concrete Dam.* Springer; 2021:129-144.
89. Lherbier JR, Andrian F. *Numerical Seismic Analysis of Pine Flat Dam Using Finite Difference Method.* Springer; 2021:145-159.
90. Menouillard T, Tzenkov A, Schwager M. *Dynamic Analysis of Pine Flat Concrete Dam: Acoustic Fluid-Structural Interaction with ANSYS Workbench.* Springer; 2021:161-174.
91. Mitovski S, Petkovski L, Kokalanov G, Kokalanov V, Panovska F. *Seismic Analysis of Pine Flat Concrete Dam.* Springer; 2021:175-189.
92. Monteiro Azevedo N, Farinha MB, Câmara R, Schlar Leitão N. *Seismic Analysis of Pine Flat Concrete Dam: Comparison of Numerical Results from 2D and 3D Analysis.* Springer; 2021:191-204.
93. Naji-Mahalleh N. *Seismic Analysis of Pine Flat Concrete Dam.* Springer; 2021:205-221.
94. Panteki E, Goldgruber M. *Seismic Excitation of a Concrete Dam: Analysis of the Influence of Modelling Approaches and Concrete Material Non-linearity.* Springer; 2021:223-235.
95. Peton P, Thénint T. *Modal, Dynamic and Seismic Analyses of the Pine Flat Concrete Gravity Dam.* Springer; 2021:237-252.
96. Robbe E, Grimal E, Devesa G. *Seismic Analyses of Pine Flat Dam: Simplified Use of Viscous Spring Boundaries and Anisotropic Damage in the Principal Directions with the Ability of Cracks Re-Closure.* Springer; 2021:253-261.
97. Salamon J, Wood C, Manie J, Geister A. *Evaluation of Seismic Wave Propagation in the Analysis of Concrete Dams: Pine Flat Dam Benchmark Study.* Springer; 2021:263-276.

98. Scolari M, Bado A, Gualco D, Buraschi L, Valsecchi R. *Finite Element Analyses of a Concrete Gravity Dam: Investigation on Static and Dynamic Behavior*. Springer; 2021:277-293.
99. Stabile A, Labbé P, Nguyen A. *Analysis of Pine Flat Dam Considering Fluid-Soil-Structure Interaction and a Linear-Equivalent Model*. Springer; 2021:295-307.
100. Staudacher EJ, Zenz G. *2D Seismic Analysis of Pine Flat Concrete Gravity Dam Including Mass of Foundation: Approach with Infinite Elements*. Springer; 2021:309-322.
101. Su W, Wang JT, Xu YJ. *Seismic Analysis of Pine Flat Concrete Dam*. Springer; 2021:323-338.
102. Valente S, He Q, Capriulo C. *Seismic Analysis of Pine Flat Concrete Dam*. Springer; 2021:339-351.
103. Vorlet S, Manso P, De Cesare G. *Seismic Behavior of Pine Flat Concrete Gravity Dam Using Microplane Damage-Plasticity Model*. Springer; 2021:353-367.
104. Yang H, Wang H, Salamon J, Jeremic B. *Earthquake Soil Structure Interaction Analysis of a Gravity Dam*. Springer; 2021:369-380.
105. Jalayer F, Cornell C. Alternative non-linear demand estimation methods for probability-based seismic assessments. *Earthquake Eng Struct Dyn*. 2009;38:951-972.
106. Applied Technology Council. Quantification of Building Seismic Performance Factors (FEMA P695, ATC-63). Tech. Rep., Washington, DC; 2009.
107. Sevieri G, De Falco A, Marmo G. Shedding Light on the Effect of Uncertainties in the Seismic Fragility Analysis of Existing Concrete Dams. *Infrastructures*. 2020;5(3):22.
108. Vamvatsikos D, Cornell C. Incremental dynamic analysis. *Earthquake Eng Struct Dyn*. 2002;31:491-514.
109. Hariri-Ardebili MA, Sattar S. Myths and Realities about ETA. *Ocean Eng*. 2021;221:108499.
110. Baker J. Efficient analytical fragility function fitting using dynamic structural analysis. *Earthq spectra*. 2015;31(1):579-599.
111. Niwa A, Clough RW. *Shaking Table Research on Concrete Dam Models*. University of California, Earthquake Engineering Research Center; 1980.
112. Donlon WP, Hall JF. Shaking table study of concrete gravity dam monoliths. *Earthquake Eng Struct Dyn*. 1991;20(8):769-786.
113. Wilcoski J, Robert R, Matheu E, Gambill J, Chowdhury M. Seismic testing of a 1/20 scale model of Koyna Dam, Report No. ERDC TR-01-17. Tech. Rep., U.S. Army Corps of Engineers, Engineering Research and Development Center; 2001.
114. Zenz G, Goldgruber M. *Proceedings of the 12th ICOLD International Benchmark Workshop on Numerical Analysis of Dams*. Austrian National Committee on Large Dams; 2013.
115. Gunn R, Balissat M, Manso P, Mouvet L, Schleiss A. *Proceedings of the 13th ICOLD International Benchmark Workshop on the Numerical Analysis of Dams*. Swiss Committee on Dams; 2015.
116. Malm R, Hassanzadeh M, Hellgren R. *Proceedings of the 14th ICOLD International Benchmark Workshop on Numerical Analysis of Dams*. KTH Royal Institute of Technology; 2017.
117. Chopra AK. *Earthquake Engineering for Concrete Dams: Analysis, Design, and Evaluation*. John Wiley & sons; 2020.

**How to cite this article:** Hariri-Ardebili MA. Quantifying modeling uncertainties in seismic analysis of dams: Insights from an international benchmark study. *Earthquake Engng Struct Dyn*. 2024;53:1168–1194.  
<https://doi.org/10.1002/eqe.4064>

## APPENDIX: DETAILED PLOTS

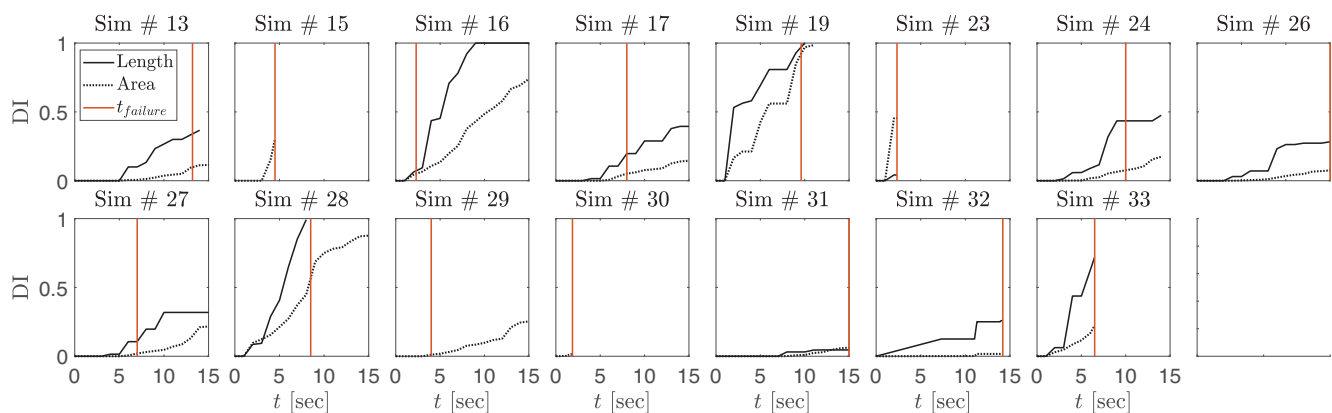


**FIGURE A1** Comparing the evolution of damage index based on length-based and area-based definitions for various participants. A same IAA is applied in all cases.

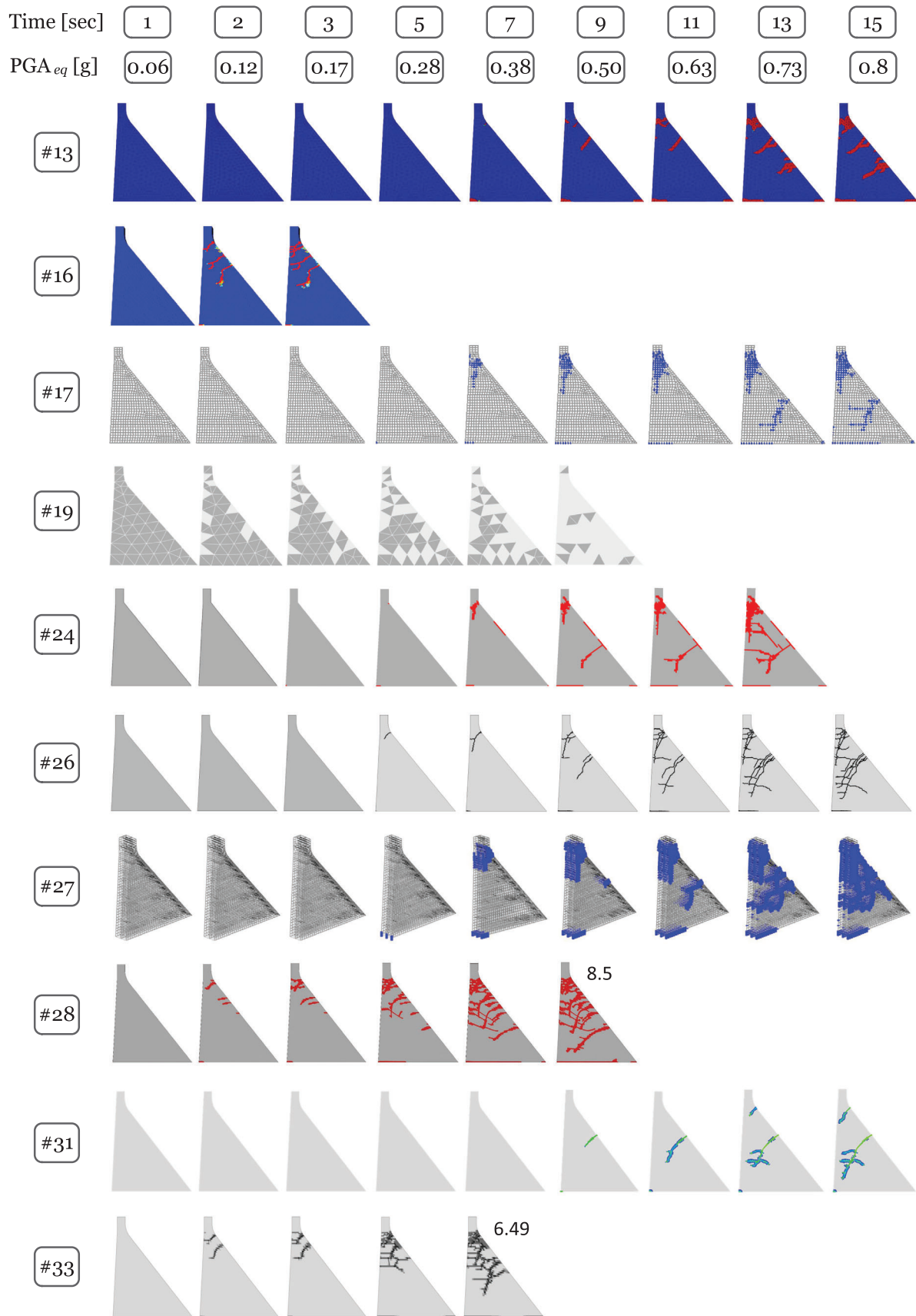


FIGURE A2 Crack propagation and failure modes of concrete dam under IAA.